FEDERAL UNIVERSITY OF SANTA CATARINA
TECHNOLOGICAL CENTER
GRADUATE PROGRAM IN MATERIALS SCIENCE AND ENGINEERING

Carolina Cotta Ramusino

Lithium disilicate glass ceramics: Effect of ion exchange and aging on structural, microstructural and optical properties

Florianópolis
2024

Carolina Cotta Ramusino

Lithium disilicate glass ceramics: Effect of ion exchange and aging on structural, microstructural and optical properties

Master's thesis presented to the Graduate Program in Materials Science and Engineering at the Federal University of Santa Catarina, as a partial requirement to obtain a title of Master in Materials Science and Engineering.

Advisor: Prof. Dr. Luciana M. Schabbach
Co-Advisor: Prof. Dr. Cláudia A.M. Volpato
Co-Advisor: Dachamir Hotza

Florianópolis
2024

Cotta Ramusino, Carolina
Lithium disilicate glass ceramics: Effect of ion exchange and aging on structural, microstructural and optical properties. / Carolina Cotta Ramusino ; orientador, Luciana Maccarini Schabbach, coorientador, Dachamir Hotza, coorientador, Cláudia Ângela Maziero Volpato, 2024.
73 p.

Dissertação (mestrado profissional) - Universidade Federal de Santa Catarina, Centro Tecnológico, Programa de Pós-Graduação em Ciência e Engenharia de Materiais, Florianópolis, 2024.

Inclui referências.

1. Ciência e Engenharia de Materiais. 2. Dissilicato de Lítio. 3. Envelhecimento. 4. Têmpera Química. 5. Translucidez. I. Maccarini Schabbach, Luciana. II. Hotza, Dachamir. III. Maziero Volpato, Cláudia Ângela IV. Universidade Federal de Santa Catarina. Programa de Pós-Graduação em Ciência e Engenharia de Materiais. V. Título.

Carolina Cotta Ramusino

The present work at the master's level was evaluated and approved by the examining board composed of the following members:

Prof. Luciana M. Schabbach, Dr.
Federal University of Santa Catarina (UFSC)
Advisor

Prof. Claudia A. M. Volpato, Dr.
Co-Advisor

Prof. Dachamir Hotza, Dr.
Co-Advisor

Prof. João Batista R. Neto, Dr.
Federal University of Santa Catarina (UFSC)
Member of the panel

Prof. Marcelo dal Bó, Dr.
Instituto Federal de Santa Catarina (IFSC)
Member of the panel

We certify that **this is the original and final version** of the final master's thesis that was considered suitable for obtaining the title of Master in Materials Science and Engineering.

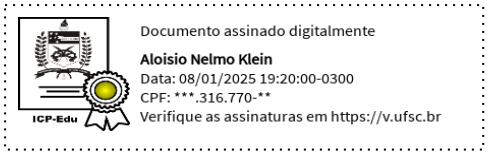

Coordinator of the Graduate Program in Materials Science and Engineering

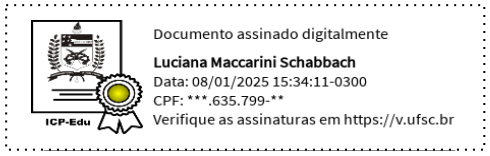

Prof. Luciana M. Schabbach, Dr.

Advisor

Florianópolis, 2024

To the Carolina of the past, who doubted her ability to succeed;
To the Carolina of the future, who is proud of the Carolina of today.
To my family and my boyfriend, who have always supported me
with unwavering love and encouragement.

ACKNOWLEDGMENTS

First of all, I would like to thank the Federal University of Santa Catarina, and all the professors involved in the Undergraduate Course in Materials Engineering at the Florianópolis Campus for all the teachings throughout this entire training period. I also thank CAPES and CNPq for funding the research scholarship.

I would like to express my gratitude to my advisor, Prof. Luciana M. Schabbach, for trusting me and our project, as well as for the support throughout this process. I am also grateful to my co-advisor, Prof. Dr. Dachamir Hotza, for embarking on this journey with me, for always being present and available, and for all the help and teachings. I would also like to thank Prof. Dr. Cláudia Ângela Maziero Volpato for giving me so much support from the beginning of my undergraduate thesis to the completion of my master's degree.

I extend my gratitude to the partnership with the Ceramic Materials Research Center (CERMAT) for keeping its doors open for the completion of this research, as well as to everyone who helped me there. I also thank the Graduate Program in Dentistry (PPGO) for providing its laboratory so that the project could be completed.

I would like to thank Prof. Dr. Marcelo Dal Bó, PhD student Wenceslau Fernandes das Neves, and the Chemistry Laboratory at IFSC (Criciúma Campus) for their assistance in carrying out the ion exchange process.

I am also grateful to my colleagues at the UFSC laboratories: Interdisciplinary Laboratory for the Development of Nanostructures (LINDEN), Central Laboratory of Electron Microscopy (LCME), X-Ray Diffraction Laboratory and Multi-User Laboratory for Physical Research (LDRX-LAMPEF-UFSC) staff for technical support during X ray diffraction experiments, especially Prof. Dr. Carlos Eduardo Maduro de Campos, for allowing the analyses present in this work to be carried out.

I want to thank my boyfriend for his unconditional support, for always being present, and for constantly encouraging me to keep moving forward and giving my best. I also thank my family for believing in me and supporting me throughout my studies.

Thank you.

"Success is not final, failure is not fatal: It is the courage to continue that counts."
– Winston Churchill

ABSTRACT

Restorations using lithium disilicate glass ceramics produced in the form of thin or ultra-thin veneers used in minimally invasive dentistry aim to preserve dental tissue but can face challenges like micro-infusion and chipping. Treatments for improve the performance of this material, including ion exchange, enhance mechanical strength, yet their impact on optical properties remains unclear. Ion exchange is a promising method that improves the mechanical behavior of ceramic materials by replacing smaller cations with larger cations, generating residual compressive stresses in the ceramic material. This technique as is well discussed in literature can enhance the mechanical strength of thin glass-ceramic samples, but its impact on optical properties is not yet well known. The present study evaluated the influence of ion exchange treatment on lithium disilicate-based ceramic samples and simulated intraoral aging through microstructural characterization and evaluation of optical behavior. Three different classes of samples were prepared: samples received no surface treatment (NT), samples had their surfaces polished (POL), and the samples were glazed (GL). All samples underwent the ion exchange treatment, and half of them were subjected to an aging protocol in a thermocycler (autoclave for 10,000 cycles). The characterization of the samples was performed through XRD, SEM, Raman, and UV-Vis analysis to evaluate the colorimetric coordinates (CIELab) and translucency parameter. The structural characterization revealed that the orthorhombic lithium disilicate ($Li_2Si_2O_5$) structure was identified for all samples, exhibiting approximately 30% crystallinity in the NT and POL groups and as low as 1% in the GL group due to the non-crystalline character of the glazing paste. Although the b-axis contraction and c-axis expansion were observed due to ion exchange and aging in NT and POL samples, these structural changes did not significantly impact the optical properties, specifically the translucency parameter (TP) and contrast ratio (CR). Raman features observed for all samples are absolutely identical. They were satisfactorily assigned as active modes of crystalline lithium disilicate, the most intense one located at 1106 cm^{-1} associated to Si-O stretching vibrations in SiO_4 tetrahedra. The EDS/SEM micrographs and Raman results indicated that there were no significant changes in the composition of the samples caused by treatment. Regarding the color was observed that, for all tested groups, with ion exchange and aging protocol, the greatest color differences were observed in the untreated group, followed by the polished and glazed groups. The GL group exhibited the highest translucency parameter (TP) after the aging process, while the NT group had the highest opacity before undergoing ion exchange (0.42) ($p<0.001$). Polishing, ion exchange, and aging were indeed capable of altering the color of the lithium disilicate samples. Nevertheless, the observed changes are within clinically acceptable ranges.

Keywords: Lithium Disilicate, Ion Exchange, Aging, Color, Translucency.

RESUMO

Restaurações usando cerâmicas vítreas de dissilicato de lítio, produzidas na forma de facetas finas ou ultrafinas utilizadas na odontologia minimamente invasiva, visam preservar o tecido dentário, mas podem enfrentar desafios como microinfiltração e lascamento. Tratamentos para melhorar o desempenho deste material, como a tempera química, aumentam a resistência mecânica, mas seu impacto nas propriedades ópticas ainda não está claro. A têmpera química é um método promissor que melhora o comportamento mecânico de materiais cerâmicos ao substituir cátions menores por cátions maiores, gerando tensões residuais de compressão no material cerâmico. Essa técnica, como bem discutido na literatura, pode aumentar a resistência mecânica de amostras finas de cerâmica vítrea, mas seu impacto nas propriedades ópticas ainda não é bem conhecido. O presente estudo avaliou a influência do tratamento de troca iônica em amostras de cerâmica à base de dissilicato de lítio e simulou o envelhecimento intraoral por meio da caracterização microestrutural e avaliação do comportamento óptico. Três grupos diferentes de amostras foram preparadas: amostras que não receberam tratamento superficial (NT), amostras que tiveram suas superfícies polidas (POL) e amostras que foram glazeadas (GL). Todas as amostras passaram por tratamento de têmpera química, e metade delas foi submetida a um protocolo de envelhecimento em uma termocicladora (autoclave por 10.000 ciclos). A caracterização das amostras foi realizada por meio de análises de XRD, SEM, Raman e UV-Vis para avaliar as coordenadas colorimétricas (CIELab) e o parâmetro de translucidez. A caracterização estrutural revelou que a estrutura ortorrômbica de dissilicato de lítio ($Li_2Si_2O_5$) foi identificada para todas as amostras, apresentando aproximadamente 30% de cristalinidade nos grupos NT e POL e apenas 1% no grupo GL devido ao caráter não cristalino da pasta de glazeamento. Embora a contração do eixo b e a expansão do eixo c tenham sido observadas devido à troca iônica e ao envelhecimento nas amostras NT e POL, essas mudanças estruturais não impactaram significativamente as propriedades ópticas, especificamente o parâmetro de translucidez (TP) e a razão de contraste (CR). As características observadas na análise Raman são idênticas para todas as amostras. Elas foram atribuídas como modos ativos do dissilicato de lítio cristalino, sendo o mais intenso localizado a 1106 cm^{-1}, associado às vibrações de alongamento Si-O nos tetraedros de SiO_4. As micrografias EDS/SEM e os resultados Raman indicaram que não houve mudanças significativas na composição das amostras causadas pelo tratamento. Em relação à cor, foi observado que, para todos os grupos testados, com o protocolo de troca iônica e envelhecimento, as maiores diferenças de cor foram observadas no grupo não tratado, seguido pelos grupos polido e vitrificado. O grupo GL exibiu o maior parâmetro de translucidez (TP) após o processo de envelhecimento, enquanto o grupo NT apresentou a maior opacidade antes de passar pela troca iônica (0,42) ($p<0,001$). O polimento, a têmpera química e o envelhecimento foram capazes de alterar a cor das amostras de dissilicato de lítio. No entanto, as mudanças observadas estão dentro de limites clinicamente aceitáveis.

Palavras-chave: Dissilicato de Lítio, Têmpera Química, Envelhecimento, Cor, Translucidez.

RESUMO EXPANDIDO

Vitrocerâmicas de dissilicato de lítio: Efeito da troca iônica e do envelhecimento na estrutura, microestrutura e nas propriedades ópticas

Introdução

Restaurações minimamente invasivas, com espessuras variando de cerca de 0,5 a 1,5 mm, têm sido cada vez mais utilizadas na odontologia com o objetivo de preservar os tecidos dentais. Essas restaurações geralmente são feitas com vitrocerâmicas por meio de técnicas de prensagem a quente ou fresagem CAD/CAM, que podem ser condicionadas com ácido hidro fluorídrico para permitir sua adesão aos tecidos dentais. Para garantir a longevidade intraoral, o material cerâmico selecionado deve ser capaz de emular as características ópticas dos tecidos dentais, bem como apresentar propriedades mecânicas favoráveis quando submetido à função oral. Entre as vitrocerâmicas disponíveis na odontologia, destacam-se a leucita, um silicato natural de alumínio e potássio do grupo dos feldspatoides, e o dissilicato de lítio. Cerâmicas à base de leucita são utilizadas para a fabricação de restaurações parciais e coroas unitárias, enquanto, devido à sua maior resistência mecânica (aproximadamente 380 MPa) em comparação à leucita (~140 MPa), o dissilicato de lítio pode ser empregado em próteses mais extensas, como próteses fixas de até 3 unidades, recomendadas para casos de perda unitária entre dois dentes saudáveis. No entanto, falhas como micro infiltração, descolamento ou fraturas podem ocorrer em restaurações feitas com espessuras finas. Para melhorar o comportamento mecânico dos materiais vitrocerâmicos, métodos de reforço como a adição de fibras ou partículas de zircônia tetragonal, têmpera térmica e troca iônica têm sido sugeridos na literatura. Entre essas técnicas, destaca-se a troca iônica, que é usada para aprimorar as propriedades mecânicas ou ópticas do material por meio da troca de íons, alterando a composição química da superfície do material. Este estudo foca em avaliar como a troca iônica, os tratamentos de superfície e o envelhecimento térmico afetam as propriedades ópticas e a microestrutura de cerâmicas de dissilicato de lítio. Essa avaliação é essencial porque a troca iônica pode causar alterações na superfície da cerâmica, que estará exposta ao ambiente oral durante o uso.

Objetivos

O principal objetivo do presente estudo é analisar o efeito da troca iônica, dos tratamentos de superfície e do protocolo de envelhecimento nas propriedades ópticas e na microestrutura de amostras de dissilicato de lítio utilizadas na Odontologia. Como objetivos específicos tem-se: avaliar se a troca iônica provoca mudanças significativas nas fases cristalinas e sua influência na cor, luminosidade, croma e matiz da vitrocerâmica; investigar como tratamentos de superfície (polimento e glazeamento) impactam as propriedades ópticas, além de analisar os efeitos da troca iônica e do envelhecimento térmico na cor e translucidez do material.

Metodologia

Blocos de dissilicato de lítio CAD/CAM (IPS e.max, Ivoclar Vivadent, Liechtenstein) foram adquiridos para esta pesquisa. Eles são fornecidos em um estado parcialmente cristalizado, conhecido como "estado azul" (Li et al., 2014). Os blocos cerâmicos foram seccionados em 45 amostras, com 1 mm de espessura cada, utilizando uma cortadora metalográfica de precisão. Após o corte, as amostras foram polidas a úmido em ambos os lados utilizando lixas abrasivas (800-1200, 3M ESPE Products, EUA). Para o tratamento superficial as amostras (n=16) foram divididas em três grupos. O grupo NT (sem tratamento) não recebeu tratamento superficial após a cristalização, e o grupo POL foi polido com borrachas abrasivas progressivas (grãos médio, fino e ultrafino; Besser, Brasil) e pasta de polimento universal (Ivoclar Vivadent, Liechtenstein) foi aplicada com um disco de feltro (Besser, Brasil) por 5 minutos. O grupo de amostras GL foi submetido à aplicação do esmalte (IPS Ivocolor Glaze Paste/FLUO, Ivoclar Vivadent, Liechtenstein). Para a realização da troca iônica as amostras foram imersas em um banho de nitrato de potássio fundido (KNO_3) a 480 ºC. Após o processo de troca iônica foi realizado um protocolo de envelhecimento. Para isso, utilizou-se uma termocicladora onde o envelhecimento das amostras foi feito por 10.000 ciclos, o que, segundo a literatura, corresponde a um tempo médio de envelhecimento de um ano de uso clínico. As amostras (separadas por grupos) foram imersas em água, com cada ciclo consistindo em 30 segundos de imersão em cada temperatura, 5°C e 55°C, totalizando 10.000 ciclos ao final do processo. Após esses tratamentos efetuou-se a caracterização das amostras. Com o objetivo de identificar e quantificar as fases cristalinas, foi realizada difração de raios X (XRD) na superfície das amostras de cada grupo e condição de tratamento, utilizando radiação Kα – Cu em um Xpert PRO MPD na faixa de 2θ de 7 a 100°, com tamanho de passo de 0,0167° e tempo de 40s por passo. A Espectroscopia Raman que permite a investigação de mudanças na polarizabilidade das ligações moleculares também foi realizada. Uma lente de ampliação de 50× foi utilizada, com uma janela espectral de 180 a 2000 cm, resolução de 6 cm para excitação com a linha de 785 nm e uma potência de laser de 300 mW por 10 segundos. A superfície e secção transversal das amostras foram observadas com Microscópio Eletrônico de Varredura e análises EDS foram conduzidas. Para analisar o comportamento óptico dos três grupos de amostras submetidos à troca iônica (antes e depois do protocolo de envelhecimento acelerado), foi utilizado um espectrofotômetro UV-Visível com esfera de integração (Minolta CM 3600d, Konica Minolta).

Resultados e Discussão

Os padrões de difração de Raios-X foram muito semelhantes para todas as amostras testadas. Além dos picos de Bragg, as amostras apresentam um halo amorfo típico, que se apresentou mais evidente nas amostras GL. Os principais picos de difração foram identificados como pertencentes à fase ortorrômbica $Li_2Si_2O_5$. Pequenas frações das fases cristalinas litiophosfato ortorrômbico Li_3O_4P, sílica SiO_2 tetragonal (cristobalita) e monoclínica e traços de silicato de magnésio hidratado $Mg_3Si_4O_{10}\cdot(OH)_2$ foram determinados na análise quantitativa de Rietveld, utilizando parâmetros estruturais das cartas COD 9012204, 1010938 e 1011152, respectivamente. A análise quantitativa das fases cristalinas pelo método de Rietveld revelou 88–100% de dissilicato de lítio, 0–10% de litiophosfato e 0–2,3% de cristobalita. A variação no teor de cada fase pode estar relacionada à aplicação não reprodutível da pasta de glazeamento na superfície das amostras. Os padrões de difração de raios X (DRX) revelaram a estrutura ortorrômbica do dissilicato de lítio ($Li_2Si_2O_5$) em todas as amostras, indicando graus de cristalinidade de aproximadamente 30% para os grupos NT e POL, e perto de 1%

para as amostras do grupo GL. De acordo com as micrografias, o envelhecimento térmico afetou a superfície das amostras, particularmente do grupo GL. O processo de troca iônica não causou alterações significativas em nenhum dos grupos (NT, POL e GL), que se assemelham às amostras não tratadas. O envelhecimento acelerado parece causar erosão nas camadas superficiais das amostras glazeadas (GL), indicando possíveis danos no esmalte aplicado devido a esse tratamento. Das análises EDS constatou-se que no grupo NT, após envelhecimento, houve aumento de oxigênio (~45%) e diminuição de sílica (~30%). No grupo POL, a sílica permaneceu quase inalterada (~30%) após troca iônica e envelhecimento. No grupo GL, o boro predominou (92,6%), indicando que o esmalte é à base de vidro borossilicato, conferindo resistência a choques térmicos e ataques químicos. Os espectros Raman das amostras exibiram duas bandas características em aproximadamente 946 cm^{-1} e 1106 cm^{-1}, atribuídas às vibrações de estiramento Si–O das unidades tetraédricas de silicato. As intensidades de outras bandas na região de 800 a 1200 cm^{-1} são muito fracas e provavelmente são causadas por imperfeições cristalinas relacionadas ao processo de cristalização utilizado para obter a fase $Li_2Si_2O_5$.A análise colorimétrica das amostras submetidas aos tratamentos revelou valores de ΔE00 ligeiramente mais baixos (1,04) após glazeamento em comparação com o estudo de Aurélio et al., no qual os autores obtiveram valores da ordem de 0,81ΔE00 para glazeamento convencional e 1,76ΔE00 para vitrificação prolongada. As diferenças de cor observadas no grupo com glazeamento podem ser atribuídas ao agente de vitrificação utilizado. Segundo o fabricante, o agente de vitrificação (IPS Ivocolor Glaze Paste/FLUO) contém vidro aluminosilicático alcalino e solvente. O aluminosilicato pode conter quantidades significativas de sódio e potássio, conhecidos como variações de feldspato. Os valores de ΔE_{00} abaixo de 1,8 são considerados aceitáveis para amostras cerâmicas, com valores entre 0,8 e 1,8 sendo classificados como uma "combinação aceitável" e abaixo de 0,8 como "excelente". No presente estudo, todos os valores de ΔE00 foram inferiores a 1,04, o que, de acordo com a classificação de Paravina et al., indica que as diferenças de cor não seriam perceptíveis clinicamente e poderiam ser consideradas clinicamente aceitáveis. Após os tratamentos de superfície, observou-se escurecimento nas amostras, especialmente após o glazeamento ($p < 0,001$), e também diminuição da luminosidade após o envelhecimento ($p = 0,043$). O grupo NT mostrou tom esverdeado após a troca iônica, enquanto os grupos POL e GL tendiam para um tom avermelhado ($p < 0,001$). As amostras também apresentaram tendência ao amarelo após os tratamentos, influenciando diretamente os valores de ΔE_{00} encontrados no estudo. Parâmetro de translucidez (TP) levemente maior foi observado no grupo GL após o envelhecimento (21,90) ($p = 0,0004$). Em relação à razão de contraste (CR), o grupo NT sem troca iônica apresentou a maior opacidade (0,42) ($p < 0,001$). Após a troca iônica, as amostras mostraram leve aumento na opacidade ($p = 0,026$), enquanto o envelhecimento não teve impacto significativo no CR das amostras ($p = 0,112$). Os grupos POL e GL demonstraram comportamento semelhante ($\alpha = 0,05$). De acordo com os resultados, o grupo não tratado apresentou a mudança mais significativa nos valores do TP e CR pós o envelhecimento, o que pode ser atribuído à falta de proteção superficial nesse grupo. Em contraste, os grupos de amostras glazeadas e polidas, especialmente o grupo glazeado, mostraram apenas pequenas variações em suas propriedades óptica TP e CR antes e após o protocolo de envelhecimento, destacando o efeito protetor desses tratamentos.

Considerações finais

Apesar das alterações de cor induzidas pela troca iônica, envelhecimento térmico e tratamentos superficiais como polimento e glazeamento, a aparência ou coloração das amostras de dissilicato de lítio permaneceram clinicamente aceitáveis. As diferenças de cor observadas (ΔE00) foram principalmente impulsionadas por variações na luminosidade (ΔL')

e matiz (ΔH'), com uma redução notável na luminosidade após a vitrificação e uma tendência geral para o amarelamento. O grupo GL após o envelhecimento apresentou a maior translucidez, enquanto o grupo NT antes da troca iônica teve a maior opacidade. Com base nos valores analisados, observou-se que a aplicação de troca iônica em facetas finas de dissilicato de lítio não alterou estrutural ou opticamente a superfície do material.
Para futuros estudos, testes mecânicos são sugeridos para verificar se as propriedades mecânicas foram alteradas pela troca iônica. O ensaio de dureza de Vickers em amostras ultrafinas de dissilicato de lítio temperadas quimicamente é sugerido para avaliar como o processo de têmpera química impacta as propriedades mecânicas da superfície do material. Além disso, uma avaliação do comportamento óptico usando o Modelo de Kubelka-Munk seria útil para fornecer espectros de transmitância e avaliar o comportamento óptico das amostras na região visível, incluindo identificar fenômenos de absorção causados pela pigmentação dos blocos de dissilicato de lítio. Recomenda-se, ainda, o uso de um protocolo de envelhecimento acelerado para simular condições de exposição à umidade, variações de temperatura e exposição aos raios UV ou de uso desse material a longo prazo.

Palavras-chave: Dissilicato de Lítio, Têmpera Química, Envelhecimento, Cor, Translucidez

LIST OF FIGURES

LIST OF TABLES

LIST OF ACRONYMS AND ABBREVIATIONS

ABNT: Brazilian Association of Technical Standards

ANOVA: Analysis of Variance

CAD: Computer-Aided Design

CAM: Computer-Aided Manufacturing

CERMAT: Center for Research in Ceramic and Composite Materials

CIELAB/CIE L*a*b*: L*a*b* Color Space

Cu-Kα: Copper-K alpha (X-ray energy, equivalent to 8.04 keV)

DRX: X-ray Diffraction

G1: Group 1, referring to samples that did not receive surface treatments

G2: Group 2, referring to samples that received polishing

G3: Group 3, referring to samples that received glazing

GL: Glazed group

HSD: Honestly Significant Difference

IFSC: Federal Institute of Santa Catarina

LCME: Central Laboratory of Electron Microscopy

LINDEN: Interdisciplinary Laboratory for the Development of Nanostructures

LMP: Precision Mechanics Laboratory

LSCnM: Laboratory of Synthesis and Characterization of Nanomaterials

MESH: Abrasive grit size (Mesh)

NT: No treatment group

POL: Polished group

PPGO: Graduate Program in Dentistry

TP: Translucency Parameter

UFSC: Federal University of Santa Catarina

LIST OF SYMBOLS

a*:	Red/green coordinate of the CIELAB color space
b*:	Yellow/blue coordinate of the CIELAB color space
L*:	Lightness corresponding to the CIELAB color space

Greek Letters

θ:	Scan angle
ΔC:	Chroma difference (a* chromaticity coordinate)
ΔE00:	Color difference
ΔH':	Hue difference (b* chromaticity coordinate)
ΔL':	Lightness difference

TABLE OF CONTENTS

1. INTRODUCTION AND OBJECTIVES

1.1 INTRODUCTION

Minimally invasive restorations, with thicknesses ranging from about 0.5 to 1.5 mm, have been increasingly used in dentistry with the aim of maintaining the dental tissues (BOMFIM et al 2020; RESENDE et al. 2018). These restorations are usually made with glass-ceramics through heat-pressing or CAD/CAM milling techniques, which can be conditioned with hydrofluoric acid to allow its adhesion to dental tissues (ÖZCAN et al 2015; PHARK et al 2022; DENRY 2010). To ensure intraoral longevity, the selected ceramic material must be able to emulate the optical characteristics of dental tissues, as well as present favorable mechanical properties when submitted to oral function (MOSHAVERINIA 2020; AWAD et al 2015).

Among the glass-ceramics available in dentistry, leucite, a natural aluminum and potassium silicate from the feldspathoid group, and lithium disilicate stand out. Leucite-based ceramics are used for the fabrication of partial restorations and single crowns, while due to its higher mechanical strength (approximately 380 MPa) compared to leucite (~140 MPa) (HALLMANN; ULMER; KERN, 2018), lithium disilicate can be employed in more extensive prostheses, such as fixed prostheses with up to 3 units, recommended for cases of single-tooth loss between two healthy teeth (MONTAZERIAN; ZANOTTO, 2017).

Combining the excellent adhesive properties of the glassy material with the monomers of the resinous dental cement, and considering the favorable mechanical behavior, variety of colors, and suitable translucency patterns, lithium disilicate has also been used in the fabrication of thin restorations such as veneers and overlays (MAGNE; STANLEY; SCHLICHTING, 2012; SCHLICHTING et al., 2011).

However, failures such as microleakage, debonding, or fractures may be present in restorations made at thin thicknesses (FOTIADOU et al., 2021). One study reported failure rates of 4.5% in thin posterior restorations made from CAD/CAM-machined blocks (ALAO et al., 2017). Yazigi et al. reported that 21% of lithium disilicate veneers with 0.8 mm thickness experienced cracks (YAZIGI; KERN; CHAAR, 2017). To minimize these failures, finishing/polishing and glazing techniques are used to provide a smoother surface for the restoration, reducing its roughness (OZEN; DEMIRKOL; PARLAR OZ, 2020). Glazing increases the surface hardness of the ceramic due to the formation of a low-expansion surface layer, as well as increasing its mechanical resistance.

To improve the mechanical behavior of glass-ceramic materials, reinforcement methods such as the addition of fibers or tetragonal zirconia particles, ceramic infiltration, thermal tempering, and ion exchange have been suggested in the literature (ALAO et al., 2017; ANSONG et al., 2013). Among these techniques, ion exchange stands out, which is used to enhance the mechanical or optical properties of the material through ion exchange, altering the chemical composition of the material's surface.

Some studies regarding the application of ion exchange are reported in literature. In 2019, Schneider analyzed the optical behavior of glass ceramics of varying thicknesses before and after ion exchange. The study showed that using ultra-thin ceramics with thicknesses ranging from 0.5 to 1.5 mm, ion exchange proved to be a promising technique, regardless of the thickness employed, showing stable optical behavior regarding color, luminosity, chroma, matrix, and translucency. In 2021, Silva analyzed the optical behavior of lithium disilicate samples fabricated with different surface treatments (such as polishing and glazing), before and after ion exchange. The tested samples showed discrete variations in color and translucency after treatments, suggesting favorable optical behavior (SILVA, 2021). Furthermore, in a review article published by Ruales-Carrera et al. (2021), focusing on the oral applications of feldspathic porcelain subjected to ion exchange, it was possible to conclude that this technique can contribute to a considerable increase in mechanical strength in glass-ceramics. In 2022 Neves observed that, after employing ion exchange using KNO_3 and $RbNO_3$, there was an increase in the flexural strength of dental feldspathic porcelains. The cationic exchange allowed for higher flexural strength values, as analyzed by the Weibull modulus, ensuring greater mechanical reliability (NEVES, 2022).

It is a consensus that improvement in mechanical properties by ion exchange process should occur without altering the translucency of the glassceramic (CESAR et al 2007; LI et al. 2023). Studies state that the increase in mechanical strength can occur without losing the material's transmittance (FISCHER et al. 2008, ŁĄCZKA et al 2015; LI et al. 2019). However, they did not provide an analysis of the translucency parameter (TP) and contrast ratio (CR) after the use of ion exchange, reinforcing the need to evaluate beyond color, these optical properties.

This study focuses on evaluating how ion exchange, surface treatments, and thermal aging affect the optical properties and microstructure of lithium disilicate ceramics. The assessment is essential because the ion exchange resulting from ion exchange can cause alterations on the ceramic surface, which will be exposed to the oral environment during use.

1.2 OBJECTIVES

1.2.1 Main Objective

The main objective of the present study is to analyze the effect of ion exchange, surface treatments, and aging protocol on the optical properties and microstructure of lithium disilicate samples used in Dentistry.

1.2.2 Specific Objectives

The specific objectives of this study are:

- Evaluate whether the treatment ion exchange causes significant changes in the presence of crystalline phases;
- Evaluate the influence of ion exchange on the color, luminosity, chroma, and hue of the studied glass ceramic;
- Investigate the influence of surface treatments (polishing and glazing) on the optical properties of the ceramic subjected to the ion exchange process;
- Evaluate the influence of ion exchange and thermal aging on color and translucency parameter (TP).

2. LITERATURE REVIEW

2.1 LITHIUM DISILICATE

Lithium disilicate is a ceramic material composed mainly of 60% to 65% lithium metasilicate crystals incorporated into a glassy matrix. Various oxides (SiO_2, Li_2O, K_2O, ZrO_2, ZnO, P_2O_5, Al_2O_3, and MgO) account for the rest of its composition (LIEN et al., 2015).

The lithium disilicate blocks for CAD/CAM machining, also used in this study, have a bluish color due to the introduction of dyes, to identify that the ceramic has undergone the partial crystallization process and is ready for machining (WILLARD; GABRIEL CHU, 2018).

Regarding its optical properties, lithium disilicate used in Dentistry is commercially available in various colors and levels of translucency. The colors range from A to D, and there is also a line for bleached teeth (AWAD et al., 2015). The translucency levels presented by lithium disilicate are three: medium opacity (MO), high (HT), and low translucency (LT) (WILLARD; GABRIEL CHU, 2018). HT ceramics have a lower quantity of lithium metasilicate crystals in the pre-crystallized phase, and LT ceramics have a higher quantity of crystals, such as lithium phosphate and lithium zinc silicate nanocrystals.

Due to the higher refractive index of light from lithium disilicate crystals compared to the glassy matrix, internal light dispersion occurs in the material leading to opacification. This phenomenon can result in increased light dispersion at the interfaces between the crystals and the matrix, resulting in increased opacity of the ceramic (SKYLLOURIOTIS; YAMAMOTO; NATHANSON, 2017). Currently, versions HO (high opacity) and MT (medium translucency) are also available.

2.2 SURFACE TREATMENTS

In order to reduce restoration abrasion and consequently bacterial adhesion on the surface, finishing and polishing have been suggested in the literature (ALAO et al., 2017; OZEN, DEMIRKOL, & OZ, 2020). Mimicking the characteristics of natural teeth can be achieved with these surface treatment techniques (polishing and glazing), as well as obtaining aesthetic properties such as shine and smoothness (AURÉLIO, DORNELES, & MAY, 2017; ALAO et al., 2017; KILINC & TURGUT, 2018).

Manual polishing of ceramics can be performed using abrasive rubbers composed of diamond particles (60 to 70 μm) dispersed in a soft elastic matrix (ALAO et al., 2017). For this procedure, the Meisinger Polishing Set (Meisinger, USA), Top Glaze (DFS Diamon GmbH, Germany), Silco-pol (DFS Diamon GmbH, Germany), Refert Polishing LiSi2 (Renfert GmbH, Germany), or Vita Suprinity Polishing Kit (VITA Zahnfabrik, Germany) are recommended (OZEN, DEMIRKOL, & OZ, 2020).

The glazing process, which aims to achieve a smooth and shiny surface, involves applying a superficial layer of a transparent enamel (glass) with low thermal expansion, providing high resistance to thermal shock and increasing the hardness of the ceramic surface (KIM et al., 2019). The commercial enamel brands typically used for CAD/CAM glazing are Optiglaze (GC America, USA), Vita Akzent Plus (VITA Zahnfabrik, Germany), and IPS Ivocolor Glaze (Ivoclar Vivadent, Liechtenstein) (OZEN, DEMIRKOL, & OZ, 2020). Glazing the surface of lithium disilicate is done by applying the glazing layer over the external surface of the prosthetic piece and subsequent heat treatment in a furnace under the heating rate and temperature conditions recommended by the manufacturer (KIM et al., 2019).

According to a study by Ozen et al. (2020), glazing is the surface treatment that showed the least color alteration from the first measurement to the final measurement (after surface treatment, adhesive cementation, and aging). However, according to some studies, finishing and polishing procedures alter the material's surface layer, which can directly interfere with the long-term optical properties of restorations (such as color stability, translucency) (KANAT-ERTURK, 2019).

2.3 ION EXCHANGE

Various reinforcement methods have been developed to enhance the mechanical behavior of feldspathic and glass-ceramic materials. Notable among these methods are the addition of fibers, the incorporation of tetragonal zirconia particles, ceramic infiltration, thermal tempering, and ion exchange. (ANUSAVICE & HOJJATIE, 1991; LEE, KON & ASAOKA, 1999; YOSHIMURA & CESAR, 2015; ARAÚJO et al., 2015).

Ion exchange, also known as chemical tempering is a diffusion process aimed at exchanging smaller radius cations for larger radius cations. (KARLSSON; JOHNSON; STÅLHANDSKE, 2010), altering the chemical composition of the surface layer (Figure 1).

One of the first patents on ion exchange performed on glass-ceramic materials was presented by Harrison P. Hood and Stanley D. Stookey of the Corning Corporation in 1957 (DONALD, 1989).

Figure 1 - Schematic representation of the ion exchange process that occurs in ion exchange.

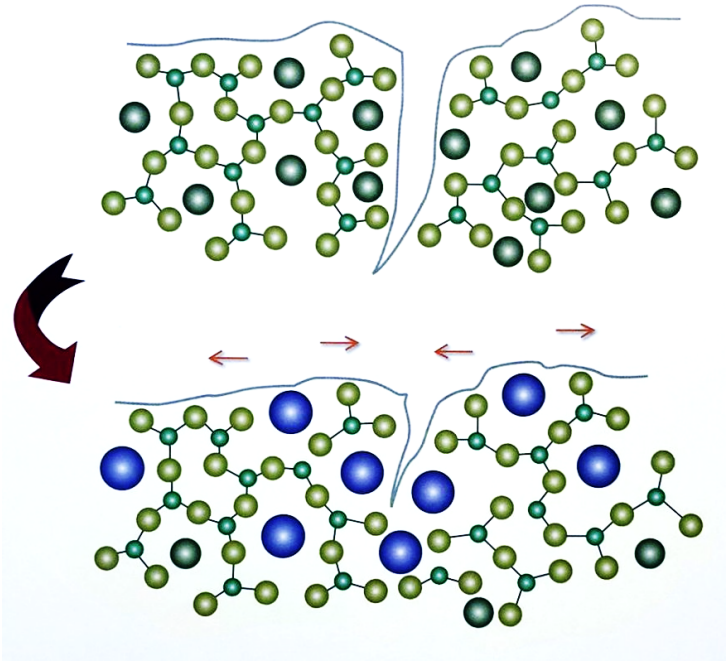

Source (Adapted from DELLA BONA, 2009).

The ion exchange process involves heating the pieces to a specific temperature in the presence of a molten salt. Temperature control is essential to avoid degradation/decomposition of the salt in use, as well as of the parts used in the treatment. Contact between the salt and the sample is maintained for a sufficient time to allow the cations of the salt, which have a larger radius, to diffuse into the surface of the part, and eventually replace the smaller-radius alkali cations (present in the material of the part) (VARSHNEYA, 2010). Among the alkali metals, the most used for the ion exchange process are presented in Figure 2, with their respective ionic diameters (pm).

Figure 2 - Ionic diameter (pm) of alkali metal cations.

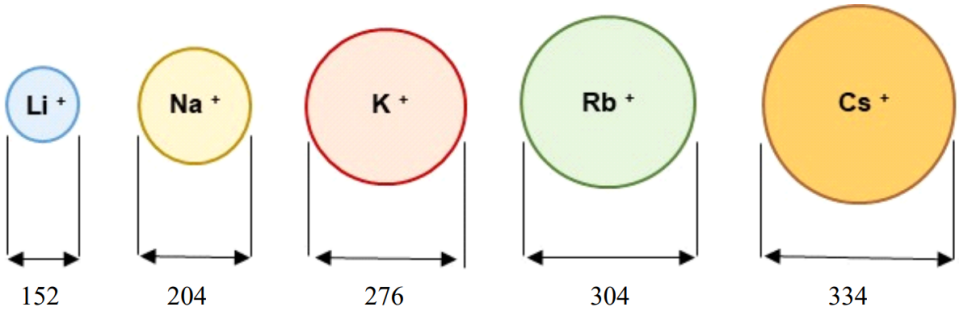

Source: (SHANNON, 1976).

For homogeneous interdiffusion (a process in which atoms diffuse into each other) upon contact with the salt on the entire surface, the chemical composition and microstructure of the involved material must be homogeneous on the surface in question. This will allow for a homogeneous depth of ion exchange, as well as a homogeneous profile of compressive stress in the cross-section of the material. On the other hand, materials with heterogeneous microstructures and chemical compositions may exhibit variations in the residual stress profile. If compression on the surface of the material is high, the increase in mechanical strength will consequently be greater (CRANK, 1979). Thus, the layer of compressive residual stress created on the material's surface can increase mechanical strength and, consequently, decrease crack propagation.

This technique typically involves Na+/K+ pairs but can also occur between Li+/Na+ or K+/Rb+ ions (ANUSAVICE, SHEN & LEE, 1992; DENRY et al., 1993; CESAR et al., 2007). Ion exchange can be achieved by two methods: soaking in a KNO_3 saline solution for 24 h or with a KNO_3 paste for 30 min at an average temperature of 470 °C, below the glass transition temperature. This temperature is chosen because the ceramic is still rigid; however, rapid ionic exchanges can occur on the material's surface.

Several studies confirm that the ion exchange process allows for the improvement of mechanical strength of feldspathic and glass-ceramic materials (DUNN, LEVY & REISBICK, 1977; ANUSAVICE, SHEN & LEE, 1992; CESAR et al., 2007; ROSA et al., 2009; ROSA et al., 2010; YOSHIMURA & CESAR, 2015), being favorable in the production of restorations in thin and ultra-thin thicknesses.

Ion exchange offers the benefit of creating a compression layer thicker than that achieved by thermal tempering and can be applied to thin ceramics as thin as 100 µm.

Additionally, it enables irregular pieces to be reinforced when the surface is in full contact with the molten salt bath (VARSHNEYA, 2010; YOSHIMURA & CESAR, 2015).

2.4 ION EXCHANGE IN DENTAL CERAMICS

Dental ceramics comprise, as a major group, feldspars (potassium and/or sodium aluminosilicates). After the heat treatment, the microstructure of these materials consists of dispersed crystalline phases in a glassy phase. To enhance mechanical properties while maintaining material aesthetics, crystalline particles are added to these materials. Thus, various types of dental ceramic compositions and different processing methods are presented.

When a layer of compressive residual stress is created on the surface of the ceramic, its mechanical strength is increased, and crack propagation is hindered (CESAR et al., 2007; ROSA et al., 2010). Several studies have confirmed that ion exchange improves the mechanical strength of feldspathic and glass-ceramic materials (CESAR et al., 2007; ROSA et al., 2010), which is favorable for minimally invasive ceramic restorations.

According to the results of a comparative study between different ceramics conducted by Cesar et al. (2007), an increase in fracture resistance (ranging from 64% to 156%) was observed after surface treatment by ion exchange. Another study evaluated samples of a glass ceramic after immersion in KNO_3 at a temperature of 450 °C for 11 h and found an increase in mechanical strength from 88.7 to 226.5 MPa, with a reduction in failure probability from 64.6% to 19.7% (FISCHER et al., 2005).

Approaches to promote ion exchange have been suggested, such as the use of molten salts like potassium hydrogen phosphate (K_2HPO_4), rubidium nitrate ($RbNO_3$), sodium nitrate ($NaNO_3$), and potassium nitrate (KNO_3). In the classical method, the ceramic material is immersed in a KNO_3 bath (Figure 3) (ROSA et al., 2010).

Figure 3 - Representation of the exchange of Na+ ions for K+ ions in ion exchange of porcelains.

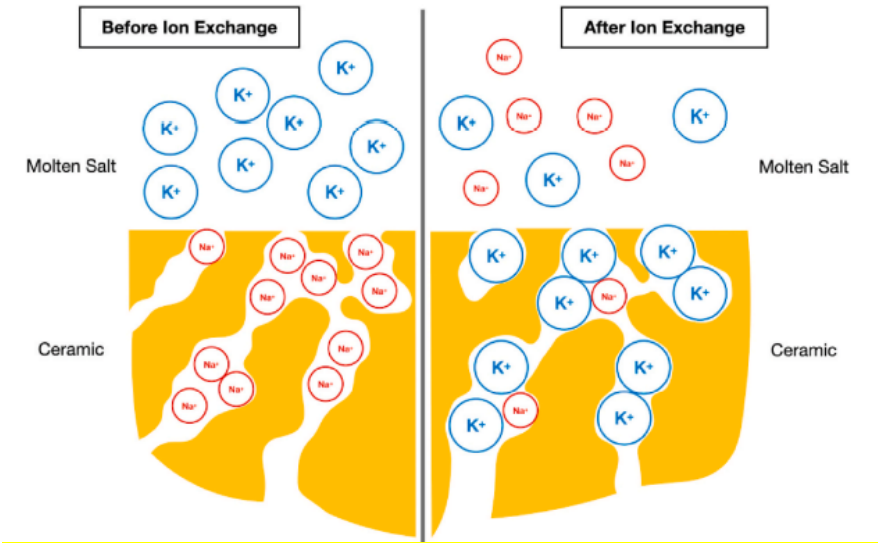

Source: (Adapted from Dunn et al. 1977)

Another method uses a paste resulting from a mixture of 10 g of KNO_3 and 4 ml of deionized water, which accelerates the chemical process (YOSHIMURA; CESAR, 2015).

3. MATERIALS AND METHODS

3.1 MATERIALS

CAD/CAM lithium disilicate blocks (IPS e.max, Ivoclar Vivadent, Liechtenstein) (Figure 4) were acquired for this research. They are supplied in a partially crystallized state, known as the "blue state" (Li et al., 2014). According to the manufacturer, various combinations of glass (usually SiO_2, Li_2O, P_2O_5, ZrO_2, ZnO, K_2O, and Al_2O_3, combined with coloring ions) are achieved using a pressure-casting procedure. The blocks consist of 40% lithium metasilicate crystals (Li_2SiO_3), in platelet form with sizes ranging from 0.2–1.0 μm, associated with lithium disilicate nuclei in a vitreous phase (VIVADENT, 2011). Additionally, the manufacturer considers the material fully crystallized after heat treatment at 850 °C for 20-25 min under vacuum (VIVADENT, 2011; LI et al., 2014). After complete crystallization, IPS e.max CAD exhibits a microstructure of 70% fine-grained lithium disilicate crystals embedded in a similar vitreous matrix (VIVADENT, 2011; WILLARD; CHU, 2018).

Figure 4 - CAD/CAM lithium disilicate blocks (IPS e.max CAD, Ivoclar Vivadent, Liechtenstein).

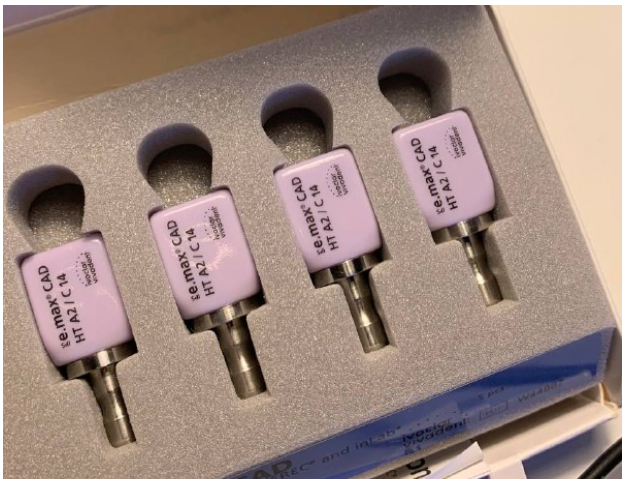

Source: elaborated by the author.

Pure lithium disilicate, according to the IPS e.max CAD scientific document, exhibits properties such as an elasticity modulus of 95 GPa when fully crystallized, and others presented in Table 1.

Table 1 - Physical properties of pure lithium disilicate. (Adapted from Ivoclar Vivadent, Schaan)

Physical properties	Partially crystallized	Fully crystallized
Biaxial strength (ISO 6872)	130 ± 30 MPa	360 ± 60 MPa
Fracture toughness (SEVNB)	0.9 – 1.25 MPa $m^{1/2}$	2.0 – 2.5 MPa $m^{1/2}$
Vickers hardness	5400 ± 200 MPa	5800 ± 200 MPa
Elastic modulus	-	95 ± 5 MPa
Coefficient of thermal expansion (100-500°C)	-	-10.45 ± 0.4 10^{-6} K^{-1}
Density	-	2.5 ± 0.1 g/cm^3
Linear expansion during tempering	0.2%	-
Chemical solubility	100 – 160 $\mu g/cm^3$	30 – 50 $\mu g/cm^3$

3.2 SAMPLE PREPARATION

3.2.1 Cutting and Finishing

The four ceramic blocks were sectioned into 45 samples with 1 mm thickness each, using a precision metallographic cutter (Isomet 1000, Leak Bluff, USA), located in the Research Laboratory of the Graduate Program in Dentistry (PPGO/UFSC). The machine was set with a lateral weight of 300 g, cutting disc position at 1.1 mm, and speed set at 350 rpm.

After cutting, the samples were wet ground on both sides using abrasive wet sandpapers (800-1200, 3M ESPE Products, USA), and the thickness of each 1 mm sample was controlled using a caliper.

After cutting, the samples were wet ground on both sides using abrasive wet sandpapers (800-1200, 3M ESPE Products, USA), and the thickness of each 1 mm sample was controlled using a caliper as shown in Figure 5.

Figure 5 - Comparison of the sample thickness (upper sample) and after (lower sample) grinding.

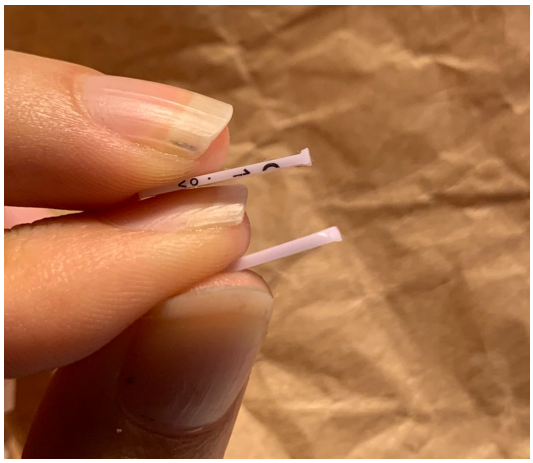

Source: elaborated by the author.

3.2.2 Heat Treatment and Surface Treatment of Samples

Next, the ground samples were taken for crystallization in a resistive electric furnace (Programat CS2, Ivoclar Vivadent, Liechtenstein), at 850 °C for 24 min. After the heat treatment, the thickness of each sample was measured again using a caliper.

The samples (n=16) were divided into three groups. The NT (no treatment) group did not receive surface treatment after crystallization, and the POL group was polished with progressive abrasive rubbers (medium, fine, and ultrafine grains; Besser, Brazil) and universal polishing paste (Ivoclar Vivadent, Liechtenstein) was applied with a felt disk (Besser, Brazil) for 5 min. The GL group was subjected to glazing (IPS Ivocolor Glaze Paste/FLUO, Ivoclar Vivadent, Liechtenstein). The glazing paste was applied to the surface of the samples with a brush according to the manufacturer's recommendations. Thereafter, the samples with the paste were placed in a furnace for 6 min and kept at 790 ˚C for 1 minute. A second layer was applied to obtain better uniformity. The same operator performed all surface treatments. The samples were cleaned with 70% vol ethanol and stored until testing.

Figure 6 - Scheme of division of sample groups regarding surface treatments. No treatment: NT, Polished: POL and Glazed: GL.

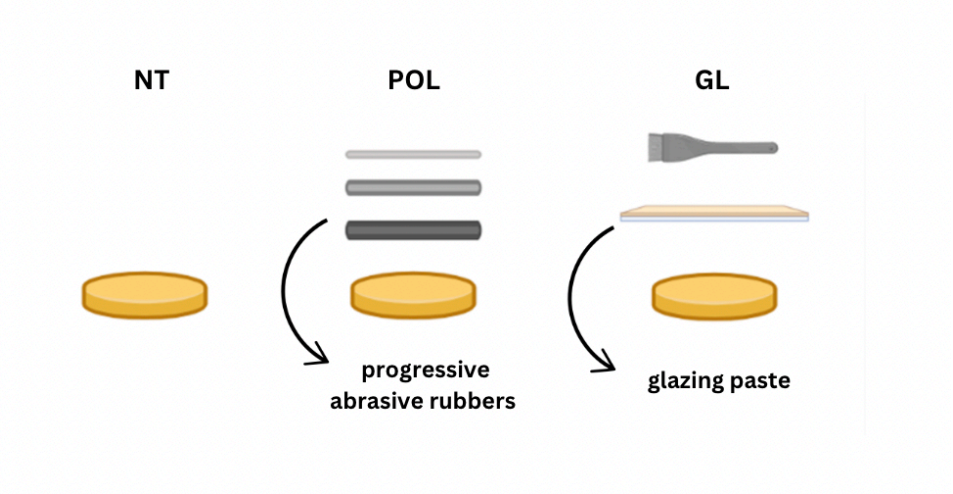

Source: elaborated by the author.

3.2.3 Ion Exchange

After the initial optical measurements, all samples (NT, POL, and GL groups) underwent the ion exchange process. This process was conducted in molten potassium nitrate (KNO_3) (Química Moderna, P.A. - ACS, 99%, Brazil) at 480 ºC for 60 min (DAL BÓ et al., 2016; FISCHER; MARX, 2001). The samples were immersed in a molten KNO_3 bath within a metal container to prevent surface contact between them.

The ion exchange was performed in an industrial oven (Sanchis, Brazil), with a heating rate of 10 °C/min. (Figure 7). To prevent thermal shock fractures, the samples were initially inserted into the furnace at 480 ºC and held at this temperature for 10 min without immersion in the molten salt. Following the 60-min chemical process, the samples were removed from the oven and allowed to cool naturally to room temperature. The surfaces were then cleaned under running water for 5 min. Finally, 92% ethyl alcohol (Êxodo Cientifica, Brazil) was used to thoroughly remove any remaining KNO3.

Figure 7 - Industrial furnace used for the ion exchange treatment (Jung, Brazil).

Source: (SILVA, 2021).

3.2.4 Aging Protocol

After the samples underwent the ion exchange process, an aging protocol was conducted. For this, a thermocycler located at the Center for Research in Ceramic Materials and Composites (CERMAT, UFSC) was used (Figure 8). The aging of the samples was carried out for 10,000 cycles. According to the literature, 10,000 cycles represent an average aging time of one year of clinical use (GALE; DARVELL, 1999).

The samples (separated by groups) were immersed in water at alternating temperatures of 5 and 55°C, with each cycle corresponding to the immersion of the samples for 30 s at each temperature, totaling 10,000 cycles at the end of the process.

Figure 8 - Thermocycler used for the aging protocol with samples immersed and separated by groups.

Source: elaborated by the author.

3.3 CHARACTERIZATION OF SAMPLES

3.3.1 X-ray Diffraction

For X-ray diffraction (XRD) analysis, in the case of polycrystals, especially with preferred orientation (as in the case of lithium disilicate), the samples are transformed into powder for greater precision. However, it is possible to perform it using samples with approximate dimensions of 1 cm^3. For this, the samples were positioned in a metal device, which should be reinforced with aluminum particles to enable the test.

Aiming to identify and quantify the crystalline phases, an X-ray diffraction (XRD) was performed on the surface of the samples from each group and treatment condition using K_α – Cu radiation in a Xpert PRO MPD (Multi-Purpose Diffractometer, Malvern Panalytical, United Kingdom) in the 2θ range from 7 to 100º with step size 0.0167° and a time of 40 s per step. The X ray diffraction measurements were performed with the Xpert MPD (MultiPurpose Diffratometer) of the LDRX-LAMPEF-UFSC.

Four scans were performed per sample (n=9) to improve data statistics. The identification of peaks in the XRD patterns was performed using the PANalytical X'Pert HighScore 2.2 software, ICDD (PDF-2), ICSD and COD databases. XRD data analyzes were performed using the Rietveld Method implemented in the TOPAS software package (COELHO, 2018). The quality of the adjustments was monitored by the agreement parameters R- weighted profile R_{wp} and Goodness of Fit GOF.

3.3.2 Raman Spectroscopy

The samples prepared for X-ray diffraction (XRD) analysis were also chemically analyzed using Raman spectroscopy, employing the PeakSeeker PRO-785 equipment (Agiltron/Raman Systems), located at LSCnM, UFSC.

The technique involves illuminating a sample with a monochromatic source (laser) and detecting the scattered light. Most of this scattered light will pass through the sample without interaction, and the detector will receive energy with the same frequency as the excitation source - this is called elastic or Rayleigh scattering. However, a small amount of light (around 0.0000001%) is scattered at different wavelengths (or colors), depending on the chemical structure, known as Raman scatter. In cases where the emitted photons have a longer wavelength than the absorbed ones, this emitted light is called "Stokes shift." This

phenomenon results from the emission of phonons to the lattice. On the other hand, "anti-Stokes shift" occurs when the emitted radiation has a shorter wavelength than the radiation used during excitation. Since this latter shift occurs when the sample emits photons with higher energy than those absorbed, it can also be called Upconversion of Energy (CAE).

In this technique, by analyzing the scattering undergone by the electromagnetic radiation after its interaction with the material (whether inorganic or organic), the identification of the material's chemical structure can be achieved. Thus, Raman spectroscopy allows for the investigation of changes in the polarizability of molecular bonds. Additionally, it enables the detection and distinction of pigments formed on the material's surface through graphs and images.

A Raman spectrum displays multiple peaks, indicating the intensity and wavelength position of scattered light. Typically, they are plotted in relation to the laser frequency, such that Rayleigh scattering is at 0 cm^{-1}. Graphs were generated for the samples under all conditions, with or without tempering, and before or after aging, along with a graph comparing all samples and conditions. When analyzing the graphs, it is important to note that the peak position in Raman spectroscopy represents the energy exchange of the incident light. The intensity of each peak depends on the distortion of electron density in the crystal due to vibration, with certain expected values for each type of crystalline structure, usually correlated with the number of bond pairs (Figure 9).

Figure 9 - Typical information from Raman Spectroscopy and corresponding material information.

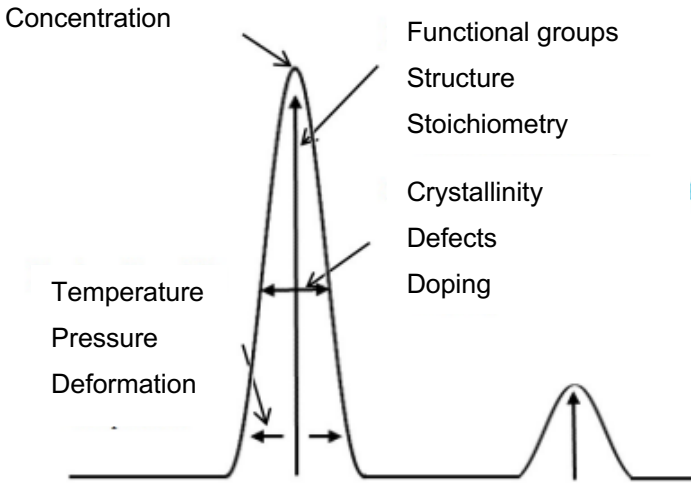

(Source: adapted from ZONGWEI, 2018).

After preparing the samples for analysis (ceramography), they were positioned near the opening of the equipment's laser (either through direct contact or point-to-point shots) to initiate the chemical analysis. A 50× magnification lens was used, with a spectral window of 180 to 2000 cm, a resolution of 6 cm for excitation with the 785 nm line, and a laser power of 300 mW for 10 s. All conditions – without tempering, with tempering before and after accelerated aging – were evaluated.

3.3.3 Scanning Electron Microscopy

The Scanning Electron Microscope (SEM) contains a source that generates a beam of electrons continuously fired at the sample during the test, performing a scanning movement on its surface. With a detector present in the equipment, it is possible to analyze the energies of the electrons during their interaction with the surface, interpreted by the equipment to generate high-definition images. However, the images generated can be obtained through secondary electrons and/or backscattered electrons. Those generated by secondary electrons, of low energy, occur through the excitation of electrons from the outermost (surface) layer of the atoms of the samples by the electron beam and serve to analyze the relief of the sample.

In the case of images generated by backscattered electrons, the high-energy ones, in addition to contrast based on relief, it is possible to obtain contrast based on the atomic number of the chemical elements present in the analyzed sample, where the lighter regions of the image represent heavier chemical elements.

After coating, the samples were taken to the microscope (SEM, Hitachi TM3030, Japan), located at LPM/UFSC.

3.3.4 Spectrophotometry UV-Vis

To analyze the optical behavior of the three sample groups subjected to ion exchange (before and after accelerated aging protocol), a UV-visible spectrophotometer with an integration sphere (Minolta CM 3600d, Konica Minolta) was used (Figure 10).

In the CIELab color space, presented in Figure 24, the colorimetric parameters L*a*b* are shown. L* represents lightness, while a* and b* represent the chromaticity coordinates. In this diagram, the a* and b* directions correspond to color directions: +a* represents the red direction, while -a* indicates the green direction. Similarly, +b* corresponds to the yellow

direction, and -b* indicates the blue direction. The central point is considered achromatic; as the values of a* and b* increase and the position moves away from the center, the color saturation increases.

Figure 10 – Representation of the CIELab system.

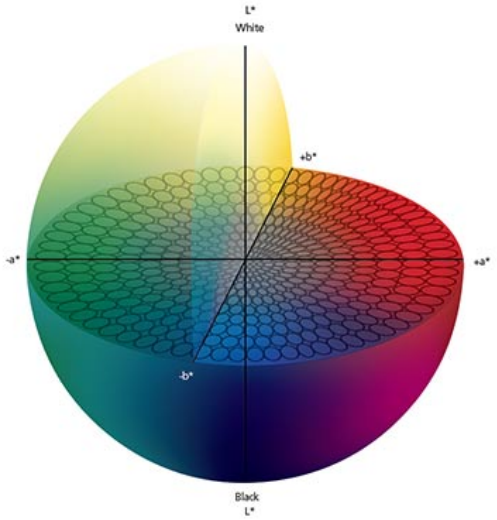

Source: Konica Minolta.

The samples, clean and dry, were placed on absolute white backgrounds, with a calibration pattern of CIE L*=92.72; a*= -1.39; b*= 4.18, and absolute black, with a pattern of CIE L*= 6.79; a*= -0.05; b*=1.45. For the analysis, reflectance mode was used with d/8° measurement geometry, a standard 2° observer, wavelengths of 360-740 nm (with a 10 nm interval), illumination/measurement area of small area (3 mm), specular component excluded (SCE), and standard illuminant D65. The L*a*b* coordinates of the CIEL*a*b* system were recorded in the system software (OnColor QC, Konica Minolta, Tokyo, Japan).

To calculate the differences in color (ΔE_{00}), luminosity ($\Delta L'$), chroma ($\Delta C'$), and hue ($\Delta H'$), the standard means of the untreated samples under an absolute white background before tempering (L*= 82.946, a*= -1.687, b*= 9.602) were compared with the means obtained from the samples of different groups (measured on the absolute white background) (Table 3). For comparison, the CIEDE 2020 formula was employed:

$$E_{00} = \left[\left(\frac{\Delta L'}{K_L S_L}\right)^2 + \left(\frac{\Delta C'}{K_C S_C}\right)^2 + \left(\frac{\Delta H'}{K_H S_H}\right)^2 + R_T\left(\frac{\Delta C'}{K_C S_C}\right)\left(\frac{\Delta H'}{K_H S_H}\right)\right]^{1/2} \quad (1)$$

where ΔL', ΔC', and ΔH' correspond to the differences in luminosity (L* coordinate), chroma (a* chromaticity coordinate), and hue (b* chromaticity coordinate). RT is the rotation function; SL, SC, and SH are weighting functions; and the parametric factors KL, KC, and KH are terms to be adjusted, which in this study were defined as 1.

To perform the measurement and ensure optical continuity, a drop of propylene glycol, a hygroscopic product with the ability to absorb water, was used between the background and the sample before each measurement. Then, the samples were measured, consecutively at their center three times, always by the same operator, in reflectance mode. It must be ensured that the sample does not move after closing the equipment's clamp, as it must remain centered to allow for correct measurement.

The translucency parameter (TP_{00}) was calculated based on the differences in L*a*b* coordinates measured on both white and black backgrounds. A higher TP00 value indicates greater translucency of the material (JOHNSTON, 1995). The following equation (Equation 1) was used to calculate TP_{00} (SALAS, 2014).

$$TP_{00} = \left[\left(\frac{L'_B - L'_W}{k_L S_L}\right)^2 + \left(\frac{C'_B - C'_W}{k_C S_C}\right)^2 + \left(\frac{H'_B - H'_W}{k_H S_H}\right)^2 + R_T\left(\frac{C'_B - C'_W}{k_C S_C}\right)\left(\frac{H'_B - H'_W}{k_H S_H}\right)\right]^{1/2} \qquad (2)$$

Where L′, C′, and H′ represent lightness, chroma, and hue, respectively, on black (b) and white (w) backgrounds. The rotation function R_T accounts for interactions between chroma and hue differences in the blue region. Weighting functions ((S_L, S_C, and S_H) adjust the overall color difference according to the specific position of the color difference pair in the L*, a*, and b* coordinates. The parametric factors (k_L, k_C, and k_H) are correction terms. The values used in the current study were $k_L = k_C = k_H = 1$ (TP_{00} (1:1:1)) (BOLT, 1994).

The differences in translucency parameters (ΔTP_{00}) were calculated by comparing initial measurements with those obtained after ion exchange and aging, using Equation 3.

$$\Delta TP_{00} = TP_{\text{after treatment}} - TP_{\text{baseline}} \qquad (3)$$

The contrast ratio (CR) was determined from measurements in the CIEXYZ system, defined as the ratio between the luminous reflectance (Y tristimulus value) on a black background (B) and that on a white background (W) (MIYAGAWA, 1981). Equation 4 was applied:

$$RC = \left(\frac{Yw}{Yb}\right) \qquad (4)$$

4. RESULTS AND DISCUSSION

4.1 STRUCTURAL AND MICROSTRUCTURAL ANALYSIS

To identify the crystal structures formed and understand their behavior after treatments such as ion exchange and aging, XRD was carried out. The identification of crystalline structures was performed by X-ray diffraction according to groups (NT, no treatment; POL, polished; GL, glazed), conditions (IE, with ion exchange; NIE, without ion exchange), and times (NA, before aging; A, after aging). The diffraction patterns are very similar for all samples tested as can be seen in Figure 11a-c. Besides the Bragg peaks all patterns as campaigned by some typical amorphous halo, are more obvious to GL samples. The main diffraction peaks were identified as being from the orthorhombic (Ccc2) $Li_2Si_2O_5$ phase (ISCD card 78562) (see Figure A1). Small fractions of orthorhombic (Pmnb) Li_3O_4P lithiophosphate, tetragonal ($P4_12_12$) SiO_2 (cristobalite) and monoclinic (C2/c) $Mg_3Si_4O_{10}{\cdot}(OH)_2$ magnesium silicate hydroxide crystalline phases were modeled in the Rietveld quantitative analysis using structural parameters from the COD cards 9012204, 1010938 and 1011152, respectively. The observation of lithium orthophosphates in almost all samples is linked to the role of this compound in the nucleation and crystallization of lithium disilicate glass (YUAN, 2014; JONG, 1994).

X-ray diffraction (XRD) analysis of the glaze paste used was also performed (Figure 12). The glaze paste, prior to heat treatment, presents an amorphous structure but with a slight tendency to crystallize yttrium silicate. Yttrium is commonly used in glaze formulations to impart fluorescence to the enamel. This analysis was conducted to verify whether the talc phase (hydrated magnesium silicate) identified could be another phase originating from the glaze, as it only appeared in the group of glazed samples.

The presence of ionic bonds in the glass can facilitate the bonding of -OH groups or fluorides to these silicates. It is likely that a small amount of magnesium silicate forms in this glass, which can easily adsorb/absorb moisture. Since the glaze is on the surface of the samples, it is highly probable that this phenomenon occurs during sample handling due to ambient moisture.

After the heat treatment the intensity of these yttrium silicate phase peaks may increase. However, no XRD analysis was performed after thermal treatment.

Figure 11 - XRD patterns: a) non-treated (NT); b) polished (POL); c) glazed (GL) samples.

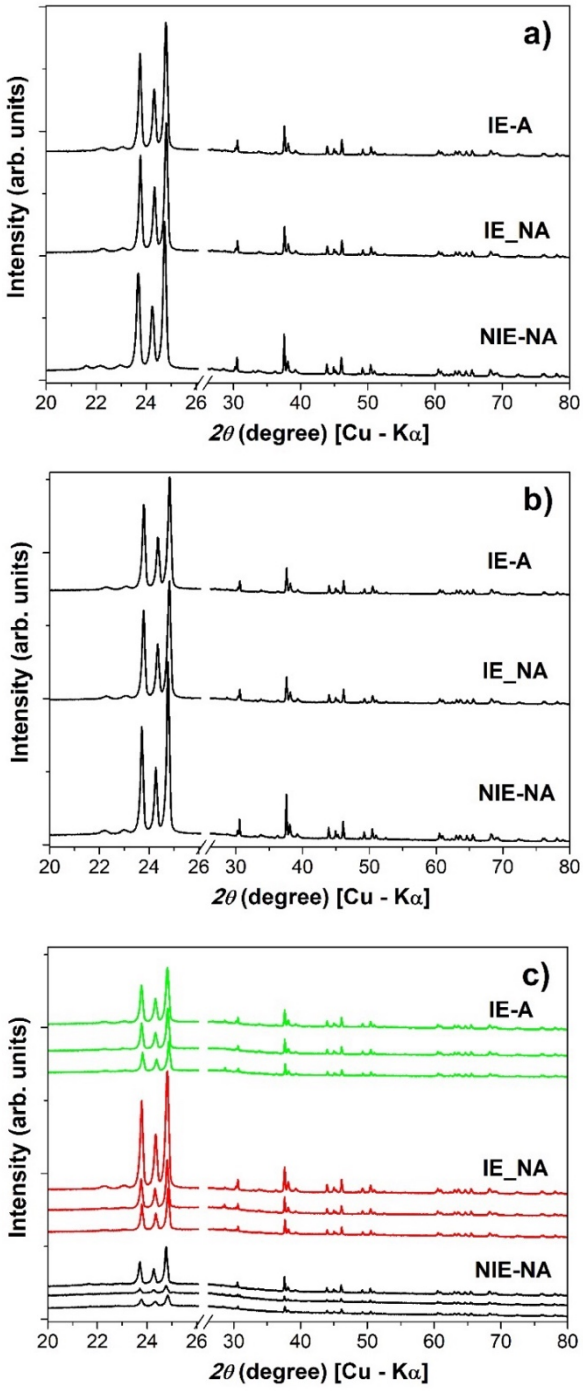

Source: elaborated by the author.

Figure 12 - XRD pattern of the glaze paste used.

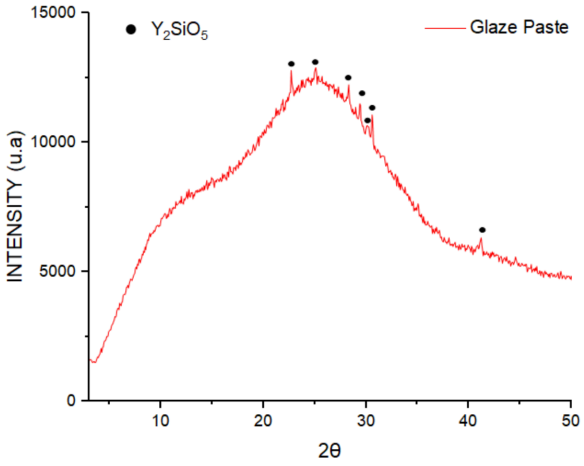

Source: elaborated by the author.

The quantitative Rietveld crystalline phase analysis revealed 88–100 % lithium disilicate, 0–10% lithiophosphate, and 0–2.3% cristobalite (see Figures 13 and 14). The range of content for each phase can be related to the non-reproducible glazing paste application (with a brush) on the surface of the samples (FISHER, 2001). No clear trend was observed for lithiophosphate content, otherwise cristobalite was not observed for POL samples. The agreement factors range from 4.1 to 8.7 for R_{wp} and 2.2 to 4.3 for GOF reinforce the visual fitting quality.

Figure 13: Experimental **(**black lines) and calculated (red lines) XRD patterns for (a) IE-A-NT, (b) IE-A-POL and (c) IE-A-GL samples. The grey lines represent the different curves concerning the black and red lines. The colored lines show the calculated pattern counterparts of each crystalline phase: lithium disilicate $Li_2Si_2O_5$ (blue), Li_3O_4P lithiophosphate (magenta), cristobalite SiO_2 (green), and magnesium silicate hydroxide $Mg_3Si_4O_{10}$ $(OH)_2$ (orange). Light grey lines represent the background fitted. Rietveld agreement factors (R_{wp} and GOF, respectively) are 8.2 and 4.1 for IE-A-NT, 8.1 and 3.9 for IE-A-POL and 5.4 and 2.6 for IE-A-GL.

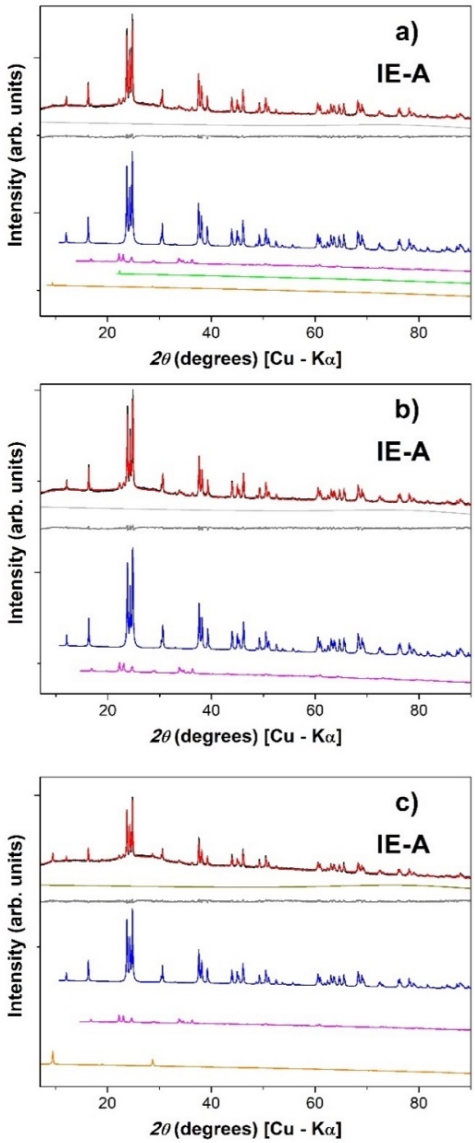

Source: elaborated by the author.

Figure 14: XRD-Rietveld quantitative phase analysis: a) non-treated (NT); b) polished (POL); c) glazed (GL) samples. The colored bars represent the crystalline phases: lithium disilicate $Li_2Si_2O_5$ (blue), Li_3O_4P lithiophosphate (magenta) and magnesium silicate hydroxide $Mg_3Si_4O_{10}$ (OH)$_2$ (orange).

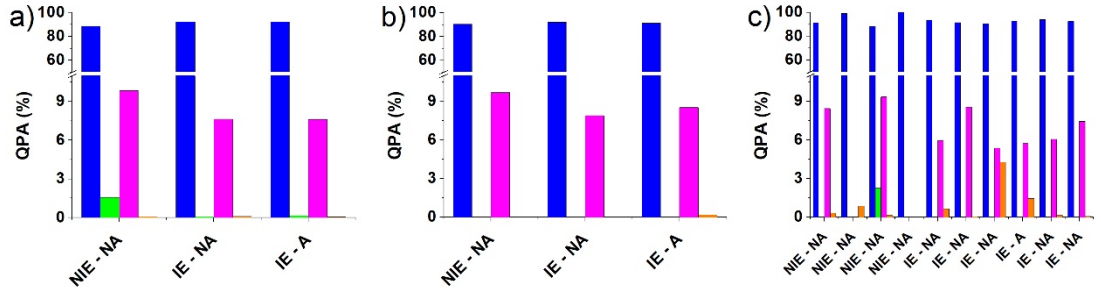

Source: elaborated by the author.

The $Li_2Si_2O_5$ cell volume showed similar values as reported at the ISCD card 78562 (JONG, 1994) and it is considerably expanded (0.7%) if compared with Paszkowicz et al. There was a slightly larger volume expansion for NIE-NA-GL samples. The lattice parameter *a* for all samples was much larger than those of both references, while *b*- and *c*-axis are contracted compared to Jong et al. It can be pointed out a clear tendency of contraction of *b*-axis and expansion of *c*-axis for the structural changes of lithium disilicate due to ion exchange and ageing for NT and POL samples (see Figure 15); these changes may indicate the replacement of lithium ions by potassium ions (of the larger size) in the structure. This behavior was not observed for GL samples that have a greater non-crystalline counterpart, due to the applied glazing paste; the vitreous phase formed tends to incorporate potassium ions from ion exchange may lead to changes in optical properties. However, $Li_2Si_2O_5$ has proven to be structurally stable in both processes. X-ray diffraction (XRD) patterns revealed the orthorhombic structure of lithium disilicate ($Li_2Si_2O_5$) in all samples, indicating degrees of crystallinity of approximately 30% for the NT and POL groups, and as low as 1% for the samples from the GL group.

Figure 15: XRD-Rietveld structural parameters of lithium disilicate $Li_2Si_2O_5$ phase: a) non-treated (NT); b) polished (POL); c) glazed (GL) samples.

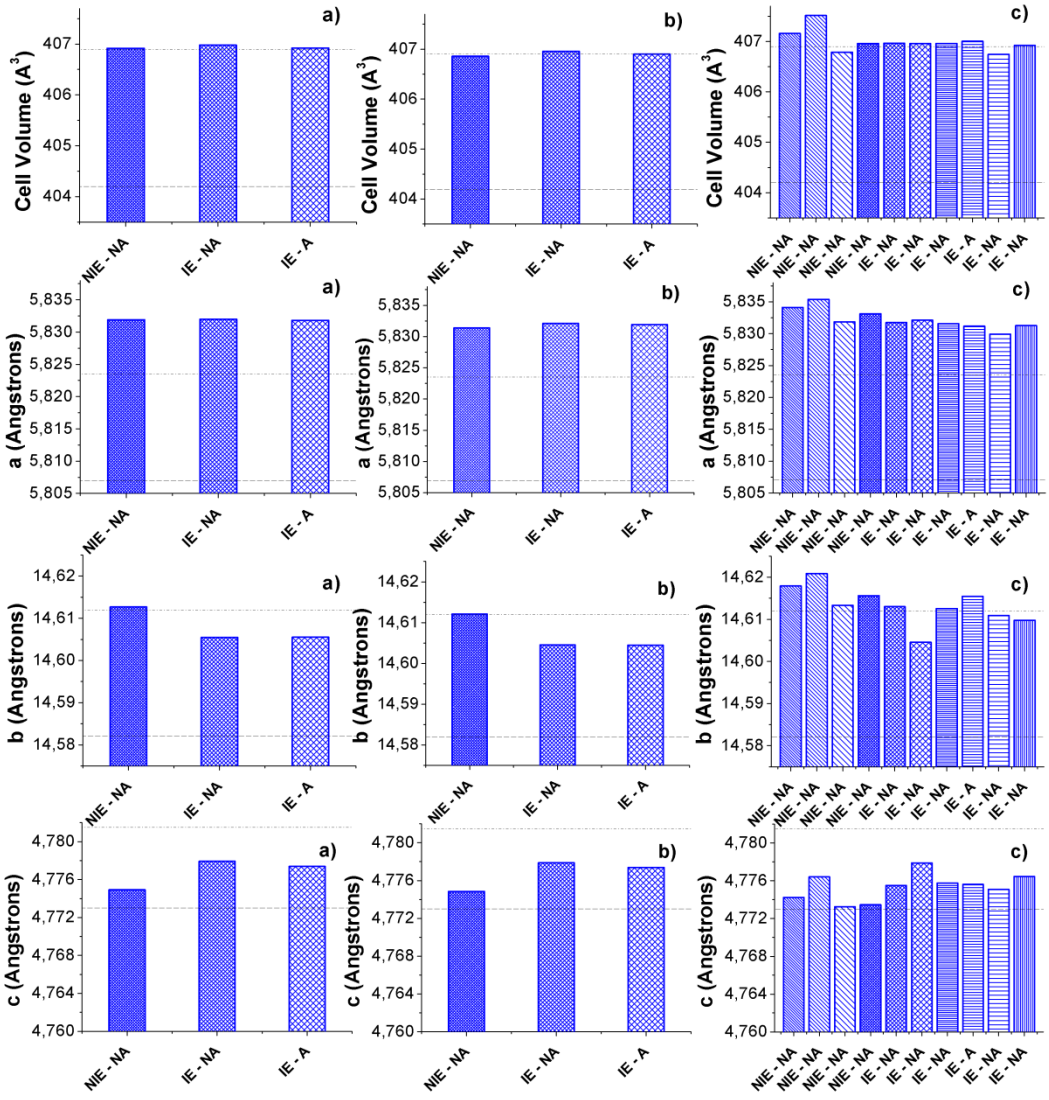

Source: elaborated by the author.

Micrographs presented in Figures 16 show the results of the morphological and topographical analysis of the material's microstructure. These images were obtained to determine whether there were any modifications on the surface of the samples after the ion exchange and the aging protocol in the tested groups. All images were taken at the center of the samples to provide a more accurate basis for comparison.

Figure 16 - Micrographs of cross-sections of the samples. Samples without ion exchange: a) NT, b) POL, and c) GL. Samples submitted to ion exchange: d) NT, e) POL, and f) GL. Samples that were aged: g) NT, h) POL, and i) GL (500× magnification).

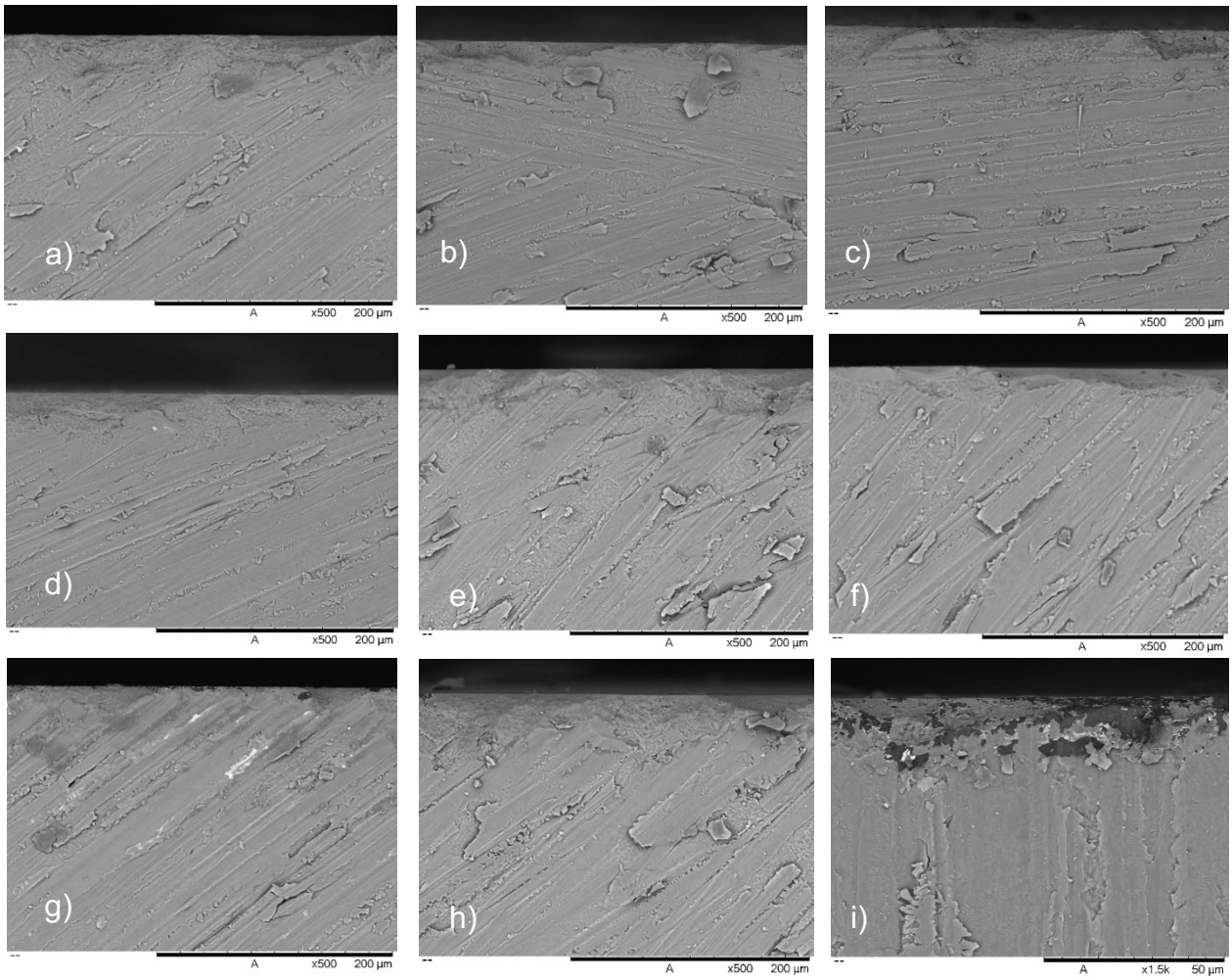

Source: elaborated by the author.

According to the micrographs, thermal aging affected the surface of the samples, particularly the GL group (Figure 16i). The ion exchange process did not cause significant alterations in any of the groups (NT, POL, and GL), as seen in micrographs 16d, 16e, and 16f, which resemble the untreated samples. Thermal aging appears to cause erosion in the surface layers of the glazed samples (GL), indicating potential damage to the applied glaze from this treatment. Figure 17 presents SEM images and EDS spectroscopy line scans (showing O, Si, K, and Na) for the NT and POL groups subjected to ion exchange and the GL group subjected to both ion exchange and aging. There is a noticeable local enrichment of O, Si, and, to some extent, K on the surface of the treated samples.

In the NT group, oxygen, aluminum, silicon, and potassium were identified in samples with and without ion exchange and aging. The majority presence of silicon and oxygen was observed. After aging, the amount of oxygen increased (~45%) while the amount of silica decreased (~30%). In the POL group, EDS also identified oxygen, aluminum, silicon, and potassium in the assessed area. After ion exchange and aging, the presence of silica remained almost unchanged (~30%). In the GL group, boron, silicon, potassium, manganese, strontium, and cerium were identified, with a majority presence of boron (92.6%), indicating that the glaze used is based on borosilicate glass. The boron acts as a fluxing agent, providing high resistance to thermal shock and chemical attack.

Figure 17 - SEM images and EDS spectroscopy line scans of groups a) NT group with ion exchange, b) POL group with ion exchange, and c) GL group with ion exchange and aging regarding O, Si, K, and Na.

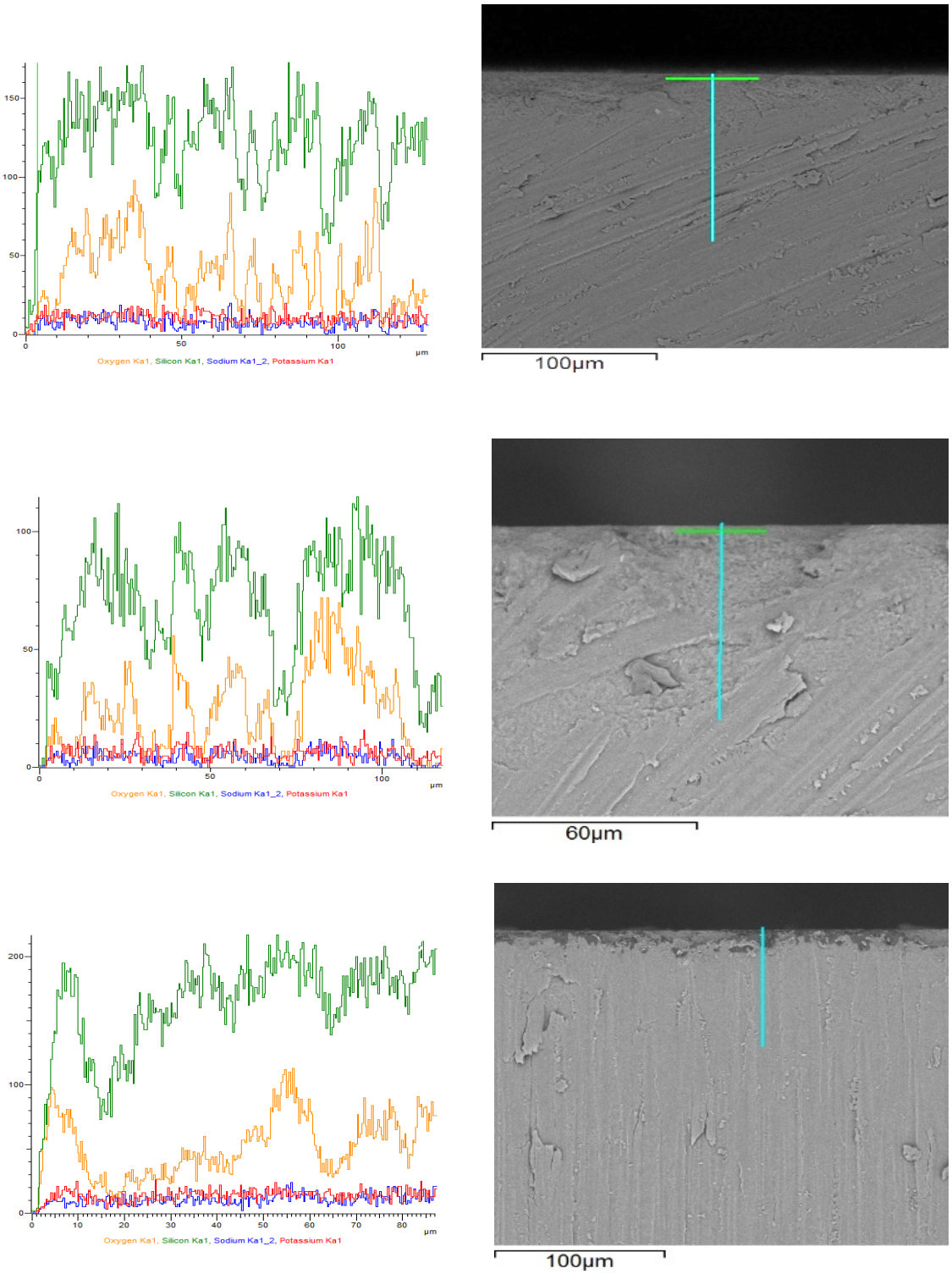

Source: elaborated by the author.

4.2 SURFACE ANALYSIS

The Raman spectra of the sample's groups in different conditions (IE and NIE) and before and after aging (NA and A) are shown in Figure 18. It is important to highlight that the unique difference in these spectra is related to the huge broad bands at high frequency. These broad bands are related to photoluminescent effects probably caused by secondary phases (crystalline and/or amorphous). All samples presented strictly the same features without any perceptive differences in height, linewidth, or center position of the peaks. This reveal that the Raman active modes observed are not sensible to the slight structural differences highlighted by the XRD results previously presented. Moreover, it can be claimed that the short-range order of lithium disilicate remains untouched by the IE and ageing processing.

Figure 18. Raman Spectroscopy spectra obtained for a) NT, b) POL and c) GL samples in different conditions (IE and NIE) and before and after aging (NA and A).

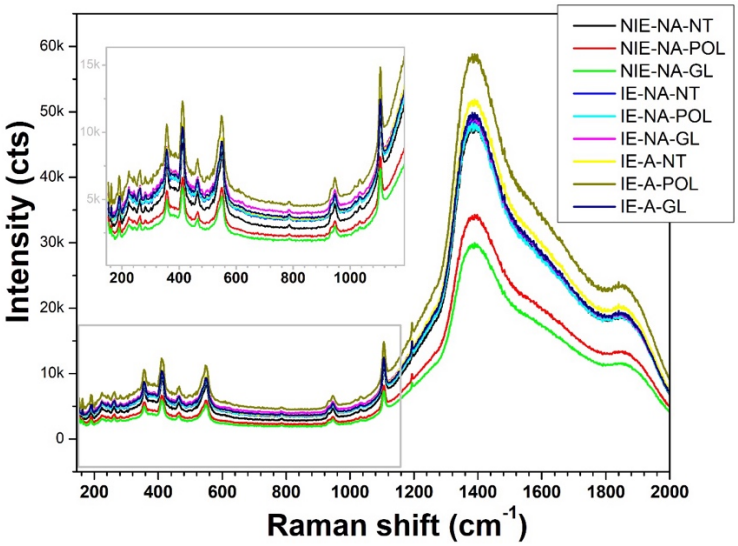

Source: elaborated by the author.

The Raman spectra of the samples exhibit two characteristic bands at approximately 946 cm^{-1} and 1106 cm^{-1}, which are attributed to Si–O stretching vibrations of tetrahedral silicate units (MILLAN, 1984). According to Sprenger's notation (SPRENGER, 1996), the structure of crystalline lithium disilicate comprises sheets of Q^3 silica tetrahedra, represented in the Raman spectra as a high-intensity $Q^3/333$ band located at 1088 cm^{-1}, as shown in Table A1. The intensities of other bands in the region from 800 to 1200 cm^{-1} are very weak and are most likely due to crystal imperfections related to the crystallization process used to obtain the $Li_2Si_2O_5$ phase (FUSS et al., 2006).

The same authors reported that a strong band at 425 cm^{-1} likely arises from rocking and symmetric bending vibrations of BO (bridging oxygen) atoms, and the main Si–O–Si symmetric stretching mode occurs at 530 cm^{-1}, as the calculated atomic motions in this mode are similar to those in ideal sheets of silica tetrahedra. Furthermore, according to the aforementioned study, Raman bands in the region from 200 to 400 cm^{-1} primarily arise from bending Si–NBO (non-bridging oxygen) vibrations (FUSS et al., 2006). In this study, we identified at least twelve features below 400 cm^{-1} and two strong bands at 412 and 550 cm^{-1} that can be interpreted in a similar manner.

4.3 OPTICAL BEHAVIOR

4.3.1 Colorimetric Analysis

After preparing the tempered samples for analysis, the average of the three measurements of the L*a*b* coordinates were obtained using a spectrophotometer, both before and after thermal aging. Table 2 presents the averages of the L*a*b* coordinates for the tempered samples of lithium disilicate before and after the accelerated aging protocol, measured against both absolute white and black backgrounds.

Table 2 - Means and standard deviations of the L* a* b* coordinates and Y tristimulus values for the groups and conditions (white and black backgrounds).

		White background				Black background			
Groups	Conditions	L*	a*	b*	Y	L*	a*	b*	Y
NT	No ion exchange	82.81 ±0.12	-1.74 ±0.03	9.70 ±0.12	61.80 ±0.22	58.08 ±0.33	-1.97 ±0.04	-0.32 ±0.15	26.04 ±0.34
	Ion exchange	82.68 ±0.09	-1.76 ±0.05	9.81 ±0.13	61.49 ±0.20	57.72 ±0.41	-1.96 ±0.04	-0.24 ±0.17	25.50 ±0.44
	Ion exchange + aging	82.45 ±0.15	-1.74 ±0.04	10.27 ±0.17	61.10 ±0.29	57.10 ±0.34	-2.03 ±0.02	-0.21 ±0.19	24.91 ±0.30
POL	No ion exchange	82.44 ±0.27	-1.78 ±0.03	9.91 ±0.06	61.01 ±0.44	56.81 ±0.27	-2.02 ±0.03	-0.23 ±0.20	24.63 ±0.23
	Ion exchange	82.04 ±0.20	-1.72 ±0.06	10.23 ±0.12	60.62 ±0.42	56.42 ±0.25	-2.00 ±0.03	-0.19 ±0.21	24.33 ±0.25
	Ion exchange + aging	81.94 ±0.35	-1.76 ±0.06	10.72 ±0.31	60.22 ±0.59	56.52 ±0.33	-2.06 ±0.04	0.02 ±0.26	24.56 ±0.39
GL	No ion exchange	81.88 ±0.13	-1.73 ±0.02	9.74 ±0.15	60.15 ±0.25	56.71 ±0.20	-1.96 ±0.04	-0.27 ±0.19	24.68 ±0.29
	Ion exchange	82.10 ±0.29	-1.69 ±0.04	9.96 ±0.17	60.45 ±0.51	56.93 ±0.41	-1.92 ±0.05	-0.17 ±0.15	24.73 ±0.45
	Ion exchange + aging	82.07 ±0.17	-1.77 ±0.04	10.59 ±0.49	60.45 ±0.27	56.34 ±0.41	-1.99 ±0.04	-0.10 ±0.29	24.25 ±0.41

Mean values and standard deviations for the differences in color (ΔE_{00}), lightness ($\Delta L'$), chroma ($\Delta C'$), and hue ($\Delta H'$) are shown in Table 3.

Table 3 - Means and standard deviations of the differences in color (ΔE_{00}), lightness ($\Delta L'$), chroma ($\Delta C'$), and hue ($\Delta H'$) for groups and conditions/time.

Groups	Conditions	ΔE_{00}	$\Delta L'$	$\Delta C'$	$\Delta H'$
NT	No ion exchange	0.16 ± 0.07^{a}	-0.14 ± 0.12^{c}	0.11 ± 0.12	0.06 ± 0.06^{e}
	Ion exchange	0.27 ± 0.07^{a}	-0.27 ± 0.09^{c}	0.23 ± 0.11	0.06 ± 0.09^{e}
	Ion exchange + aging	0.58 ± 0.14	-0.50 ± 0.15	0.67 ± 0.16	-0.09 ± 0.08
POL	No ion exchange	0.43 ± 0.15^{a}	-0.51 ± 0.27^{c}	0.33 ± 0.05	0.05 ± 0.05^{e}
	Ion exchange	0.75 ± 0.14^{b}	-0.90 ± 0.20^{d}	0.62 ± 0.10	-0.11 ± 0.11^{f}
	Ion exchange + aging	1.04 ± 0.26	-1.01 ± 0.35	1.11 ± 0.30	-0.17 ± 0.12
GL	No ion exchange	0.74 ± 0.09^{b}	-1.07 ± 0.13^{d}	0.15 ± 0.14	0.02 ± 0.05^{e}
	Ion exchange	0.63 ± 0.21^{b}	-0.14 ± 0.12^{d}	0.34 ± 0.15	-0.09 ± 0.09^{f}
	Ion exchange + aging	0.93 ± 0.25	-0.88 ± 0.17	0.99 ± 0.48	-0.12 ± 0.11

*Statistical similarities are identified by equal superscript letters ($\alpha = 0.05$).

The present study found ΔE_{00} values to be slightly lower after glazing (Table 3) when compared with the study by Aurélio et al., in which the authors obtained values in the order of $0.81\Delta E_{00}$ for conventional glazing and $1.76\Delta E_{00}$ for extended glazing. In a study that used the CIELab system, the color differences found for the group with glazing were $2.64\Delta E_{ab}$ when compared with a polished group ($5.72\Delta E_{ab}$) and with the control group ($4.24\Delta E_{ab}$) (OZEN, 2020). Another study also found color differences in polished and glazed ceramic samples after immersion in tea (1.50 and $3.03\Delta E_{ab}$, respectively) and coffee (0.68 and $3.76\Delta E_{ab}$, respectively) (KANAT, 2019).

The color differences observed in the group with glazing may be attributed to the glazing agent used. According to the manufacturer, the glazing agent (IPS Ivocolor Glaze Paste/FLUO) contains alkaline aluminosilicate glass and solvent. Aluminosilicate can contain significant amounts of sodium and potassium, known as feldspar variations (CARRERA, 2022). Additionally, the presence of large alumina crystals (about 4 μm) is directly related to the material's opacity (MIYAGAWA; POWERS; O'BRIEN, 1981).

The ΔE00 values found also suggest that the ion exchange process was capable of altering the color of the samples, particularly in the NT and POL groups ($p=0.0001$). Ion exchange is a chemical process that creates a compressive residual stress layer on the material's surface, thereby enhancing its mechanical stability against the nucleation of surface cracks (CARRERA, 2022). Besides improving the mechanical strength of the material, this process can result in the release of elements or alterations in the microstructural surface topography (MIYAGAWA; POWERS; O'BRIEN, 1981), which may affect light reflection and consequently, color perception and stability (AWAD, 2015).

In the present study, the greatest ΔE00 values were found in the POL (1.04) and GL (0.93) groups after aging ($p<0.001$). Interactions between the groups and aging were not identified ($p=0.98$). After aging or acid attack, selective ion leaching may induce a degree of corrosion degradation in an aqueous environment (MILLEDING; HARALDSSON; KARLSSON, 2002). According to Palla et al. (2018), the rough surface might have facilitated water penetration and the consequent silica network dissolution, resulting in a reduction of crystallinity and greater absorption of coloring pigments. Conversely, pressed vitrified ceramics prevent water penetration and silica network dissolution due to the absence of surface irregularities and microcracks.

For a comprehensive evaluation of color differences in dentistry, perceptibility and acceptability thresholds serve as pivotal quality control tools, aiding in the determination of clinically acceptable disparities. These thresholds not only facilitate the selection of

appropriate esthetic dental materials but also aid in the interpretation of visual and instrumental findings in both clinical and in vitro research settings. Derived from clinical research conducted in vivo, these thresholds provide a crucial clinical reference point (PARAVINA, PÉREZ, GHINEA, 2019; PARAVINA, 2015). The perceptibility threshold signifies the smallest difference in color detected by an observer, with a 50:50% ratio indicating that 50% of individuals perceive the difference while the other 50% do not (PARAVINA, 2015). Similarly, the acceptability threshold denotes the point at which 50% of individuals classify the observed color difference as acceptable, thus establishing a standard for clinical acceptability (PARAVINA, PÉREZ, GHINEA, 2019; PARAVINA, 2015).

Reference values for ΔE00 of 0.8 (for the perceptibility threshold) and 1.8 (for the acceptability threshold) are recommended by the literature when the CIEDE2000 formula is used to evaluate ceramic samples, as well as the classification of the following types of optical incompatibility: moderately unacceptable ($1.8 < \Delta E00 \leq 3.6$), clearly unacceptable ($3.6 < \Delta E00 \leq 5.4$), and extremely unacceptable ($\Delta E00 > 5.4$) (PARAVINA, PÉREZ, GHINEA, 2019; PARAVINA, 2015). Thus, it is worth noting that all values of ΔE00 color differences found in the present study were less than 1.04 ΔE00. Still, according to this classification, ΔE00 values between 0.8 and 1.8 are considered an "acceptable match," while ΔE00 values below 0.8 are considered an "excellent match." If the results found are compared with the clinical thresholds recommended by Paravina et al., the ΔE00 value found in the present study would not be clinically perceived and could be considered clinically acceptable (PARAVINA, PÉREZ, GHINEA, 2019; PARAVINA, 2015). Additionally, ΔE00 between conditions tested (before ion-exchange: T0, after ion-exchange: T1, and after aging: T2) were presented in Figure 19. It is observed that aging causes a considerable increase in the differences (ΔE00) observed in the samples when compared with the other samples.

Figure 19 - Color differences (ΔE_{00}) for the comparations between conditions tested.

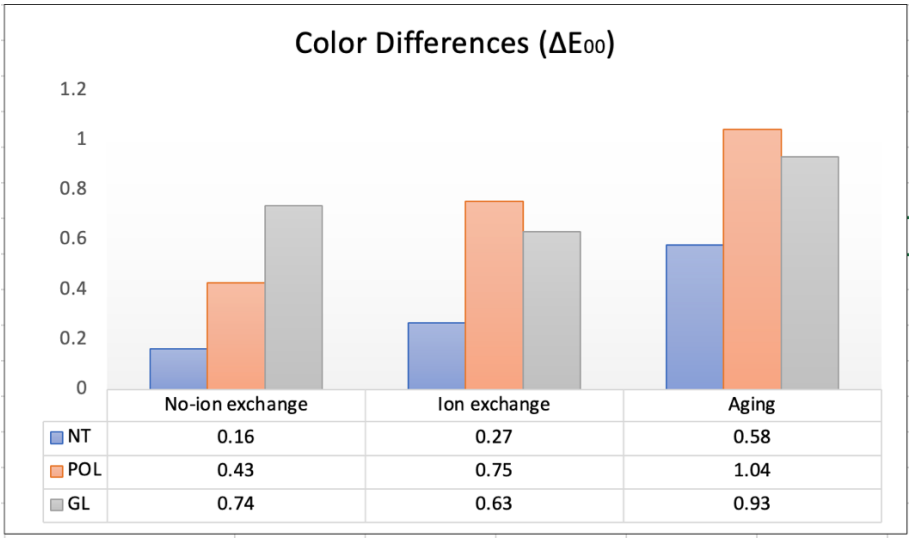

Source: elaborated by the author.

The lightness, chroma and hue differences were also analyzed in the tested ceramic samples. Multifactorial ANOVA for *Groups X Ion Exchange* and *Groups X Time* can be found in Table 4.

Table 4 - Multifactorial ANOVA for lightness (ΔL'), chroma (ΔC') and hue differences (ΔH') in relation to groups (no treatment, polishing and glazing), conditions (with and without ion exchange) and time (before and after aging).

	ΔL’									
	Groups × Conditions					Groups × Time				
Variation factor	df	SS	MS	F	p	df	SS	MS	F	p
1st variable	2	5.890	2.94	75.755	<0.001	2	3.745	1.873	36.629	<0.001
2nd variable	1	0.156	0.156	4.004	0.050	1	0.218	0.218	4.272	0.043
Interactions	2	0.943	0.471	12.126	<0.001	2	0.102	0.051	0.999	0.374
Error	54	2.099	0.039			54	2.761	0.051		
Total	59	9.089				59	6.826			
	ΔC’									
	Groups × Conditions					Groups × Time				
Variation factor	df	SS	MS	F	p	df	SS	MS	F	p
1st variable	2	1.021	0.511	37.282	<0.001	2	1.740	0.870	13.229	<0.001
2nd variable	1	0.596	0.596	43.497	<0.001	1	4.115	4.115	62.563	<0.001
Interactions	2	0.072	0.072	2.625	0.081	2	0.114	0.057	0.866	0.426
Error	54	0.739	0.014			54	3.551	0.0657		
Total	59	2.428				59	9.521			
	ΔH’									
	Groups × Conditions					Groups × Time				
Variation factor	df	SS	MS	F	p	df	SS	MS	F	p
1st variable	2	0.107	0.005	8.441	<0.001	2	0.167	0.081	7.780	0.001
2nd variable	1	0.116	0.116	18.425	<0.001	1	0.097	0.097	9.333	0.003
Interactions	2	0.064	0.032	5.039	0.009	2	0.036	0.018	1.719	0.188
Error	54	0.341	0.006			54	0.565	0.010		
Total	59	0.628				59	0.861			

After surface treatments, a decrease in the lightness of the samples, indicating a darkening effect, was observed, particularly after glazing ($p < 0.001$). Furthermore, lightness also decreased in the groups following aging ($p = 0.043$), compared to the "after ion exchange" condition. Tukey's HSD test revealed a similar behavior ($p = 0.42$) between the POL and GL groups after aging ($\alpha = 0.05$). Although changes (ΔL’) in lightness were also observed after ion exchange, they were not statistically significant ($p = 0.050$).

In terms of chroma, the NT group samples exhibited a more greenish hue after ion exchange. Conversely, the samples from the POL and GL groups tended towards redness ($p < 0.001$). However, Tukey's HSD test did not find similar statistical behavior in ΔC' ($p = 0.001$). When examining the behavior of the a* coordinate after aging (Table 2), the numerical values closely resembled those of the initial condition of each group (before ion exchange), suggesting that chroma variations were minimal and likely not responsible for the ΔE00 color differences observed after aging.

Regarding hue, the samples exhibited a tendency towards yellow after surface treatments ($p < 0.001$), after ion exchange ($p < 0.001$), and after aging ($p = 0.003$), underscoring the direct influence of this parameter on the ΔE00 values found in the present study. Tukey's HSD test revealed a similar behavior between the POL and GL groups before and after ion exchange ($p = 0.97$) and after aging ($p = 0.50$) ($\alpha = 0.05$). Studies evaluating glass ceramics have reported similar findings in polished and glazed groups, demonstrating a tendency towards darkening and yellowing (AURÉLIO, 2017; YILMAZ, 2014).

4.3.2 Translucency Analysis

The translucency parameter (TP) was determined from the differences between the L*a*b* coordinates on absolute white and black backgrounds. The higher the value obtained, the greater the material's translucency. The translucency parameter (TP_{00}) and contrast ratio (CR) results exhibited significant differences among the groups ($p < 0.001$) and with aging ($p = 0.0004$). Figures 20a and 20b illustrate the behavior of the translucency parameter (TP) and the contrast ratio (CR). The highest TP was observed in the GL group after aging (21.90) ($p = 0.0004$). In terms of CR, the NT group without ion exchange showed the highest opacity (0.42) ($p < 0.001$). Following ion exchange, the samples displayed increased opacity ($p = 0.026$), while aging did not significantly impact the CR of the samples ($p = 0.112$). The POL and GL groups demonstrated similar behavior ($\alpha = 0.05$).

Figure 20. Translucency parameters (TP) and contrast ratio (CR) for the samples analyzed.

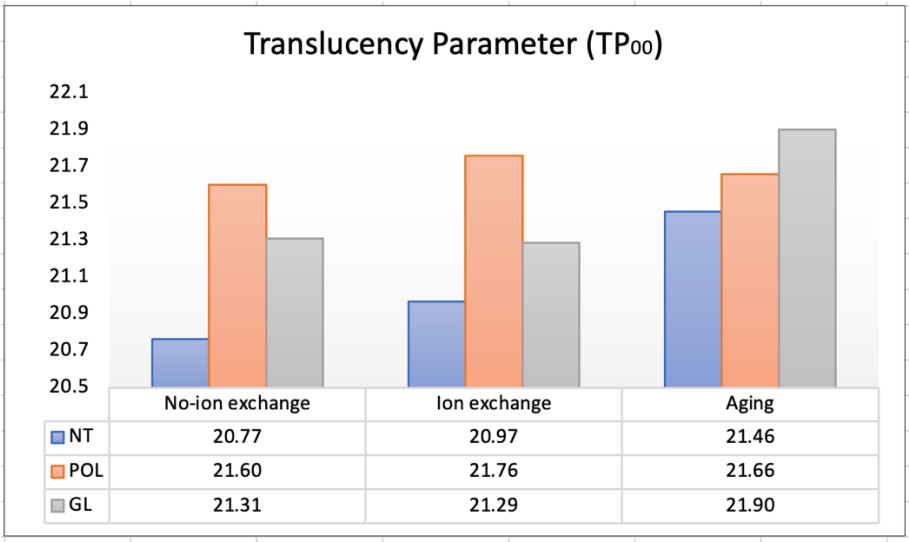

Source: elaborated by the author

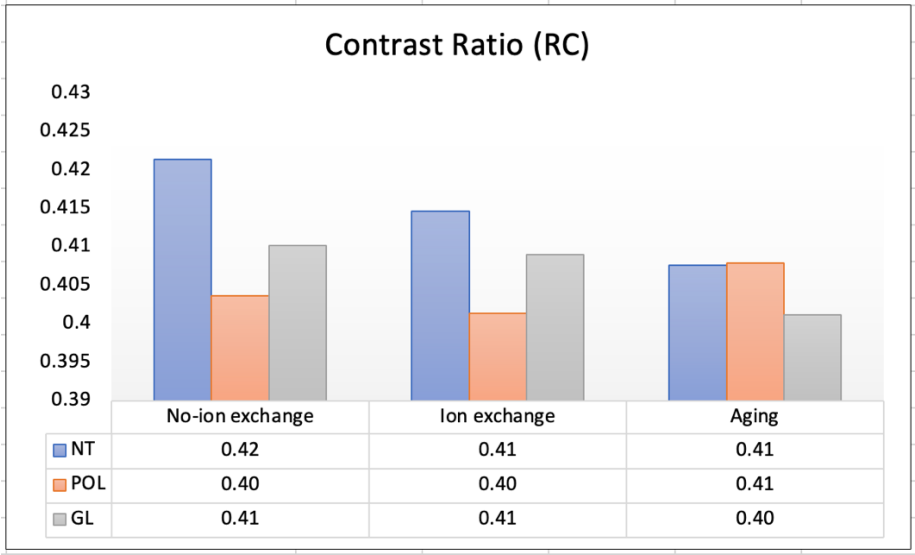

Source: elaborated by the author.

The translucency parameter (TP_{00}) and contrast ratio (CR) can be influenced by several factors, including the crystalline structure of the ceramic, grain size, presence of pigments, porosity, and the size, number, and distribution of defects within the ceramic (AWAD, 2015). In glass ceramics, there is an inverse relationship between translucency and the degree of crystallinity. Regarding roughness, irregular surfaces reflect and scatter incident light more diffusely, thereby reducing translucency (ALP, 2018). After the crystallization process, lithium disilicate glass-ceramics typically have a crystal size of approximately 1.5

μm (JONG, 1994). Ceramic materials composed of small particles (approximately 0.1 μm in diameter) can present translucency, while ceramic materials with larger particles (approximately 10 μm in diameter) allow reflection and absorption of light when it falls on the surface of the material having an opaque appearance (AWAD, 2015).

Comparing the initial translucency parameter values of the NT, POL, and GL groups with the values found after ion exchange and aging, the following translucency parameter differences (ΔTP00) were observed: 0.20±0.33 and -0.69±0.39 for the NT groups after ion exchange and aging, respectively; 0.16±0.31 and 0.06±0.41 for the POL groups; and -0.03±0.47 and 0.59±0.52 for the GL groups, respectively. According to the literature, ΔTP00 values can be correlated with the 50:50% translucency perceptibility (TPT00) and acceptability thresholds (TAT00), emphasizing the importance of obtaining translucency data through this parameter (TP) to simulate in vivo conditions (SALAS, 2018). ΔTP00 values between >0.6 and ≤2.6 indicate acceptable match behavior, while values ≤0.6 indicate excellent match behavior. In the present study, despite the numerical changes in translucency across the groups and time points tested, the differences found are considered clinically acceptable according to the recommended thresholds.

The additional the heat treatment employed during glazing may also be related to the color and translucency differences found in this study. Beyond the initial crystallization process to which all samples were subjected, the glazed samples underwent an additional heating cycle after applying two layers of the glazing agent. Changes in the heat treatment process can affect the size of the lithium disilicate crystals, thereby influencing the colorimetric behavior and degree of translucency of the ceramic (BAI, 2017). High temperatures or continuous exposure to heat can also impact the optical properties of glass ceramics, as temperature variations can lead to recrystallization and devitrification of the ceramic (AURÉLIO 2017, YILMAZ, 2014).

Studies have reported that ion exchange did not influence the translucency of glass ceramics; however, these studies did not perform specific optical tests for TP evaluation (LI, 2023, FISCHER, 2008). During ion exchange, sodium ions are replaced by potassium ions at a temperature 100°C below the glass transition temperature, by immersing the samples in a saline KNO3 solution bath (ROSA, 1981; CESAR 2007; ROSA, 2009). In the present study, the translucency of the lithium disilicate samples did not show significant differences ($p = 0.18$) after the ion exchange. This is likely because the ion exchange process only affected the outermost surface layer of the ceramic (approximately 50 to 100 μm) (FISHER, 2005), and thus did not significantly alter the TP and CR (KIM, 2019).

It is worth noting that higher mean values indicate greater translucency of the samples. According to the results, the untreated group exhibited the most significant change in values after aging. This may be due to the lack of surface protection in this group. In contrast, the glazed and polished sample groups, especially the glazed group, showed only slight variations in their means before and after the aging protocol, highlighting the protective effect of these treatments.

The TP values were analyzed by two-way ANOVA (treatments and aging), as presented in Table 5. Subsequently, the statistical differences found were compared by Tukey's test (α=0.05).

Table 5 - Two-way ANOVA for the translucency parameter (TP) in relation to the groups and times employed.

Factor	**SS**	**df**	**MS**	**F**	**P**
Groups	1.62	2	0.81	4.7	0.012
Aging	2.80	1	2.80	16.4	<0.001
Groups x Aging	2.13	2	1.06	6.2	0.003
Error	9.24	54	0.17	-	-
Total	15.79	59	-	-	-

Concerning the translucency parameter (PT), the groups, aging, and interactions proved to be significant (values in red). Thus, Tukey's Honestly Significant Difference (HSD) test (α=0.05) was used to identify the differences found (Tables 6 to 8).

Table 6 - Tukey's HSD multiple comparisons test for the translucency parameter (TP) in relation to the tested groups.

Groups	**Values**
ST	27.22
GLAZ	27.50
POL	27. 61

* The vertical bar indicates statistical similarity (p=0.102).

It can be observed that the glazed and polished sample groups appeared more translucent, and statistically, more similar.

Table 7 - Tukey HSD multiple comparisons test for translucency parameter (TP) in relation to aging.

Groups	**Values**
Without aging	27.23
With aging	27.66

Table 8 - Tukey HSD multiple comparisons test for the translucency parameter (TP) concerning the interactions between groups and aging.

Groups	Aging	Values
ST	Without	26.89
GLAZ	Without	27.13
ST	With	27.55
POL	With	27.57
POL	Without	27.66
GLAZ	With	27.87

* The vertical bar indicates statistical similarity (p=0.102).

In Table 8, it is noticeable that the untreated group without aging showed a lower translucency value. However, for all other groups, with or without the protocol, they presented statistically similar values, with higher translucency.

5. CONCLUSIONS AND PERSPECTIVES

Despite the alterations in color induced by ion exchange, thermal aging, and surface treatments such as polishing and glazing, the changes in the lithium disilicate samples remained clinically acceptable. The orthorhombic lithium disilicate ($Li_2Si_2O_5$) structure was consistently identified across all samples, exhibiting approximately 30% crystallinity in the NT and POL groups and as low as 1% in the GL group. Although the b-axis contraction and c-axis expansion were observed due to ion exchange and aging in NT and POL samples, these structural changes did not significantly impact the optical properties, specifically the translucency parameter (TP) and contrast ratio (CR). The observed color differences (ΔE00) were primarily driven by variations in lightness (ΔL') and hue (ΔH'). A noticeable reduction in lightness was observed after glazing, accompanied by a general tendency towards yellowing after all treatments. Notably, the aged GL group exhibited the highest translucency, while the NT group before ion exchange demonstrated the greatest opacity.

Based on the presented and analyzed values, it can be observed that the application of ion exchange on thin lithium disilicate facets did not structurally and optically alter the material's surface. However, for future work, mechanical tests are suggested to verify if mechanical properties were altered using ion exchange. In ultrathin samples with surface treatment, mechanical strength can be significantly affected, making it essential to perform hardness tests, such as the Vickers test, to quantify these improvements or identify potential weaknesses. The Vickers hardness test on chemically tempered ultrathin lithium disilicate samples is necessary to evaluate how the tempering process impacts the mechanical properties of the material's surface. Additionally, regarding the optical properties, a complete analysis using Kubelka-Munk Model would be useful to provide transmittance spectra and evaluate the optical behavior of the samples in the visible region, including identifying possible absorption phenomena caused by pigmentation of lithium disilicate blocks.

Moreover, the use of an accelerated aging protocol is recommended to simulate long-term exposure conditions. This protocol can help predict how the material’s translucency, color stability, and structural integrity may change over time, especially under environmental stressors like humidity, temperature fluctuations, and UV exposure. Such insights are essential for understanding the material's durability and performance in real-life applications.

REFERENCES

ALAO, A. R. et al. Fracture, roughness and phase transformation in CAD/CAM milling and subsequent surface treatments of lithium metasilicate/disilicate glass-ceramics. Journal of Mechanical Behavior of Biomedical Materials, v. 74, p. 251-260, 2017.

ANSONG, R. et al. Fracture toughness of heat-pressed and layered ceramics. The Journal of Prosthetic Dentistry, v. 109, n. 4, p. 234-240, 2013.

ANUSAVICE, K. J.; HOJJATIE, B. Effect of thermal tempering on strength and crack propagation behavior of feldspathic porcelains. Journal of Dental Research, v. 70, p. 1009-1013, 1991.

ARAÚJO, M. D. et al. Effect of fiber addition on slow crack growth of a dental porcelain. Journal of Mechanical Behavior of Biomedical Materials, v. 44, p. 85-95, 2015.

AURÉLIO, I. L.; DORNELES, L. S.; MAY, L. G. Extended glaze firing on ceramics for hard machining: Crack healing, residual stresses, optical and microstructural aspects. Dental Materials, v. 33, p. 226-240, 2017.

AWAD D., STAWARCZYK B., LIEBERMANN A., NICOLETA I., Translucency of esthetic dental restorative CAD/CAM materials and composite resins with respect to thickness and surface roughness, J. Prosthet. Dent. 113 (2015) 534-540.

BOLT R.A., BOSCH J.J., COOPS J.C., Influence of window size in small-window color measurement, particularly of teeth, Phys. Med. Biol. 39 (1994) 1133-42. https://doi.org/10.1088/0031-9155/39/7/006

BOMFIM, D. I.; RAHIM, N. M.; AUSTIN, R. S. Biomechanical planning for minimally invasive indirect restorations. British Dental Journal, v. 229, p. 425-429, 2020.

CARRERA, E. R. et al. Chemical tempering of feldspathic porcelain for dentistry applications: A review. Open Ceramics, v. 6, p. 100201, 2022. https://doi.org/10.1016/j.oceram.2021.100201.

CESAR P.F., GONZAGA C.C., MIRANDA W.G., YOSHIMURA H.N., Effect of ion exchange on hardness and fracture toughness of dental porcelains, J. Biomed. Mater. Res. B Appl. 83 (2007) 538-545. HYPERLINK "https://doi.org/10.1038/s41415-020-2170-x" https://doi.org/10.1002/jbm.b.30826

COELHO, A. A. TOPAS and TOPAS-Academic: An optimization program integrating computer algebra and crystallographic objects written in C++. Journal of Applied Crystallography, v. 51, p. 210-218, 2018. https://doi.org/10.1107/S1600576718000183.

CRANK, J. The mathematics of diffusion. Oxford: Oxford University Press, 1979. ISBN 0198534116.

DAL BÓ, M. et al. Chemical tempering of porcelain tiles. Ceramics International, v. 42, p. 15199-15202, 2016. https://doi.org/10.1016/j.ceramint.2016.06.138.

DERY I., HOLLOWAY J.A., Ceramics for dental applications: a review, Materials. 3 (2010) 351-368. https://doi.org/110.3390/ma3010351.

DENRY, I. L. et al. Enhanced chemical strengthening of feldspathic dental porcelain. Journal of Dental Research, v. 72, p. 1429-1433, 1993.

DONALD, I. W. Methods for improving the mechanical properties of oxide glasses. Journal of Materials Science, v. 24, n. 12, p. 4177-4208, 1989. https://doi.org/10.1007/BF02385824.

FISCHER, H.; MARX, R. Improvement of strength parameters of a leucite-reinforced glass ceramic by dual-ion exchange. Journal of Dental Research, v. 80, p. 336-339, 2001. https://doi.org/10.1177/00220345010800010701.

FISCHER H., DE SOUZA R.A., WÄTJEN A.M., RICHTER S., EDELHOFF D., MAYER J., MARTIN M., TELLE R., Chemical strengthening of a dental lithium disilicate glass-ceramic

material, J. Biomed. Mater. Res. 87 (2008) 582-587. HYPERLINK "https://doi.org/%2010.2341/17-007-T" https://doi.org/10.1002/jbm.a.31798

FOTIADOU, C. et al. Longevity of lithium disilicate indirect restorations in posterior teeth prepared by undergraduate students: A retrospective study up to 8.5 years. Journal of Dentistry, v. 105, p. 103569, 2012. https://doi.org/10.1016/j.jdent.2012.11.014.

FUSS, T. et al. Ex situ XRD, TEM, IR, Raman and NMR spectroscopy of crystallization of lithium disilicate glass at high pressure. Journal of Non-Crystalline Solids, v. 352, p. 38-39, 2006. https://doi.org/10.1016/j.jnoncrysol.2006.01.040.

GALE, M. S.; DARVELL, B. W. Thermal cycling procedures for laboratory testing of dental restorations. Journal of Dentistry, v. 27, n. 2, p. 89-99, 1999.

GASPARIK C., CULIC B., VARVARA M.A., GRECU A., BURDE A., DUDEA D., Effect of accelerated staining and bleaching on chairside CAD/CAM materials with high and low translucency. Dent. Mater. J. 38 (2019) 987-93. https://doi.org/10.4012/dmj.2018-335

HALLMANN, J.; ULMER, P.; KERN, M. Effect of microstructure on the mechanical properties of lithium disilicate glass-ceramics. Journal of Mechanical Behavior of Biomedical Materials, v. 82, p. 355-370, 2018.

JOHNSTON W.M., MA T., KIENLE B.H., Translucency parameter of colorants for maxillofacial prostheses, Int. J. Prosthodont. 8 (1995) 79-86.

JONG, B. D.; SLAATS, P. G. G.; SUPER, H. T. J.; VELDMAN, N.; SPEK, A. L. Extended structures in crystalline phyllosilicates: Silica ring systems in lithium, rubidium, cesium, and cesium/lithium phyllosilicate. Journal of Non-Crystalline Solids, v. 176, p. 164-171, 1994. https://doi.org/10.1016/0022-3093(94)90074-4.

KANAT-ERTÜRK, B. Color stability of CAD/CAM ceramics prepared with different surface finishing procedures. Journal of Prosthodontics, v. 29, p. 166-172, 2019.

KARLSSON, S.; JONSON, B.; STÅLHANDSKE, C. The technology of chemical glass strengthening – A review. European Journal of Glass Science and Technology Part A, v. 51, p. 41-54, 2010.

KILINC, H.; TURGUT, S. Optical behaviors of esthetic CAD-CAM restorations after different surface finishing and polishing procedures and UV aging: An in vitro study. Journal of Prosthetic Dentistry, v. 120, p. 107-113, 2018.

KIM, S. J. et al. Color changes of ceramic veneers following glazing with respect to their composition. Journal of Advanced Prosthodontics, v. 11, p. 16-22, 2019.

KRUGER, H.; KAHLENBERG, V.; KAINDL, R. Li2Si3O7: Crystal structure and Raman spectroscopy. Journal of Solid State Chemistry, v. 180, n. 5, p. 922-930, 2006.

ŁĄCZKA K., CHOLEWA-KOWALSKA K., SRODA M., RYSZ J., MARZEC M.M., ŁĄCZKA M., Glass-ceramics of LAS (Li2O–Al2O3–SiO2) system enhanced by ion-exchange in KNO3 salt bath, J. Non-Cryst. Solids. 428 (2015) 90-97. HYPERLINK "https://doi.org/%2010.2341/17-007-T" https://doi.org/10.1016/j.jnoncrysol.2015.08.003

LE PEVELEN, D. D. Encyclopedia of Spectroscopy and Spectrometry. N. I.: Elsevier, 2017.

LEE, H. H.; KON, M.; ASAOKA, K. Fracture toughness and durability of chemically or thermally tempered metal-ceramic porcelain. Biomedical Materials and Engineering, v. 9, p. 135-143, 1999.

LI, R. W.; CHOW, T. W.; MATINLINNA, J. P. Ceramic dental biomaterials and CAD/CAM technology: State of the art. Journal of Prosthodontic Research, v. 58, p. 208-216, 2014.

LI X.C., CHEN Z.X., LI D., LIU W.Z., MENG M., Chemical and mechanical stability of an ion-exchanged lithium disilicate glass in artificial saliva, J. Mech. Beh. Biomed. Mater. (2023) 105563. HYPERLINK "https://doi.org/%2010.2341/17-007-T" https://doi.org/10.1016/j.jmbbm.2022.105563.

LI X.C., LI D., MENG M., WEI R., HE L., ZHANG S.F., Significant strengthening of a lithium disilicate glass by Li+/Na+ exchange at substantially lowered temperature, Ceram. Int. 45 (2019) 22665-22674. HYPERLINK "https://doi.org/10.1038/s41415-020-2170-x" https://doi.org/10.1016/j.ceramint.2019.07.300.

MAGNE, P.; STANLEY, K.; SCHLICHTING, L. H. Modeling of ultrathin occlusal veneers. Dental Materials, v. 28, p. 777-782, 2012.

MILLAN, P. Structural studies of silicate glasses and melts - Applications and limitations of Raman spectroscopy. American Mineralogist, v. 69, p. 622-644, 1984. https://doi.org/10.2138/am-1984-5-612.

MILLING, P.; HARALDSSON, C.; KARLSSON, S. Ion leaching from dental ceramics during static in vitro corrosion testing. Journal of Biomedical Materials Research, v. 61, p. 541-550, 2002. https://doi.org/10.1002/jbm.10109.

MIYAGAWA, Y.; POWERS, J. M.; O'BRIEN, W. J. Mechanical properties of dental ceramics: Strengthening mechanisms. Journal of Dental Research, v. 60, p. 1345-1349, 1981. https://doi.org/10.1177/00220345810600110601.

MIYAGAWA, Y.; POWERS, J. M.; O'BRIEN, W. J. Strengthening of dental ceramics by ion exchange. Journal of Dental Research, v. 59, p. 991-994, 1980. https://doi.org/10.1177/00220345800590070501.

MOORHEAD, J. R. et al. An in vitro analysis of filler particle effects on the compressive strength and modulus of commercial resin-matrix ceramics. The Journal of Prosthetic Dentistry, v. 116, n. 3, p. 410-417, 2016. https://doi.org/10.1016/j.prosdent.2016.01.024.

MOSHAVERINIA A., Review of the modern dental ceramic restorative materials for esthetic dentistry in the minimally invasive age, Dent. Clin. North. Am. 64 (2020) 621-631. https://doi.org/10.1016/j.cden.2020.05.002.

MUKHERJEE, S. L. R. Engineering design and analysis of a CAD/CAM glass ceramic. Biomaterials, v. 9, p. 188-190, 1988.

NAM, K.; LIM, M. Mechanical properties of a newly developed lithium disilicate glass ceramic for dental restorations. Journal of Mechanical Behavior of Biomedical Materials, v. 23, p. 97-107, 2013.

NEVES, W. F.das. Estudo da influência do processo de têmpera química sobre as propriedades mecânicas de porcelanas odontológicas feldspáticas ultrafinas. 2022. 145 f. Tese (Doutorado) - Curso de Pós Graduação de Engenharia Mecânica, Universidade Federal de Santa Catarina, Florianópolis, 2022.

OKAZAKI, M. In vitro durability of ion exchanged glass-ceramics for dental use. Journal of Biomedical Materials Research, v. 8, p. 557-564, 1974. https://doi.org/10.1002/jbm.820080609.

OTTO, T.; PFEFFER, S. Effect of surface treatment and aging on bond strength of CAD/CAM-fabricated lithium disilicate ceramic and dentin cemented with universal adhesives. Journal of Prosthetic Dentistry, v. 121, p. 233-241, 2019. https://doi.org/10.1016/j.prosdent.2018.03.022.

ÖZCAN M., VOLPATO C.A.M., Surface conditioning protocol for the adhesion of resin-based materials to glassy matrix ceramics: how to condition and why? J. Adhes. Dent. 17 (2015) 292-293. https://doi.org/10.3290/j.jad.a34590

PAZIN, M. G.; CULIOLI, M.; MIRANDA, G. A. The effect of accelerated aging and thermal cycling on the mechanical properties of different lithium disilicate ceramics. Dental Materials, v. 37, p. 1070-1080, 2021.

PHARK J.H., DUARTE JR S., Microstructural considerations for novel lithium disilicate glass ceramics: A review, J. Esthetic Rest. Dent. 34 (2022) 92-103. https://doi.org/10.1111/jerd.12864

PORATH, L.; KLAUER, K. F.; DECKER, G. Chemically toughened alumino-silicate glass for dental use. Journal of Biomedical Materials Research, v. 10, p. 225-238, 1976. https://doi.org/10.1002/jbm.820100207.

RAMP, L. C. et al. Flexural strength of lithium disilicate and zirconia core ceramics: An in vitro study. The Journal of Prosthetic Dentistry, v. 96, p. 233-238, 2006. https://doi.org/10.1016/j.prosdent.2006.08.004.

RESENDE T.H., REIS K.R. , L.H., SCHLICHTING, MAGNE P., Ultrathin CAD-CAM ceramic occlusal veneers and anterior bilaminar veneers for the treatment of moderate dental biocorrosion: A 1.5-year follow-up, Oper. Dent. 43 (2018) 337-346. https://doi.org/10.2341/17-007-T.

ROSSI, E. et al. Influence of etching time on the resin cement bond to lithium disilicate glass ceramic. Operative Dentistry, v. 46, p. E37-E44, 2021. https://doi.org/10.2341/20-097-L.

ROSSO, M. et al. Crystallization behavior and physical properties of lithium disilicate glass-ceramics in the SiO2-Li2O-K2O-ZrO2 system. Journal of Non-Crystalline Solids, v. 404, p. 124-129, 2014. https://doi.org/10.1016/j.jnoncrysol.2014.07.034.

SALAS M., LUCENA C., HERRERA L.J., YEBRA A., DELLA BONA A., PERÉZ M.M., Translucency thresholds for dental materials, Dent. Mater. 43 (2018) 1168-74. https://doi.org/10.1016/j.dental.2018.05.001

SCHNEIDER, L. F. Avaliação da estabilidade de cor de uma resina nanocerâmica submetida a intervenções de higiene e imersão em café. 2020. 69 f. TCC (Graduação) - Curso de Odontologia, Universidade Federal de Santa Catarina, Florianópolis, 2020.

SILVA, L. H.; SAKURAI, H.; OLIVEIRA, M. D. Effect of surface treatments on the shear bond strength between a resin cement and an alumina-based ceramic. Journal of Prosthetic Dentistry, v. 94, p. 601-607, 2005. https://doi.org/10.1016/j.prosdent.2005.10.011.

SILVA, R. K. e. Efeito da têmpera química na cor e translucidez de amostras finas de dissilicato de lítio. 2021. 81 f. Dissertação (Mestrado) - Curso de Programa de Pós-Graduação em Odontologia, Odontologia, Universidade Federal de Santa Catarina, Florianópolis, 2021.

SOARES, F. Z. et al. Effect of chemical tempering on flexural strength of two glass-ceramics. Dental Materials, v. 30, p. e236-e242, 2014. https://doi.org/10.1016/j.dental.2014.07.013.

TATE, R. F. et al. The effect of glaze and polishing on the flexural strength of a lithium disilicate glass-ceramic. Journal of Prosthetic Dentistry, v. 113, p. 159-167, 2015. https://doi.org/10.1016/j.prosdent.2014.08.009.

TEPPE, C.; DREWS, J.; RASMUSSEN, M. T. Influence of glaze application techniques on the flexural strength and surface roughness of two CAD/CAM ceramics. The Journal of Prosthetic Dentistry, v. 118, p. 227-232, 2017. https://doi.org/10.1016/j.prosdent.2016.10.032.

VALLITTU, P. K.; EKENDAHL, A. E. Fracture resistance of monolithic and bilayer CAD/CAM lithium disilicate crowns after fatigue loading. Journal of Prosthetic Dentistry, v. 111, p. 142-147, 2014. https://doi.org/10.1016/j.prosdent.2013.06.018.

WANG, X. et al. Residual stresses in dental glass-ceramics: Effects of machining and crystallization processes. Journal of the European Ceramic Society, v. 40, p. 2307-2315, 2020. https://doi.org/10.1016/j.jeurceramsoc.2020.01.055.

WANG, X.; HÖLAND, W.; WEGNER, R. J. Residual stresses in a dental glass-ceramic: Generation and implications for strength. Dental Materials, v. 27, p. 737-744, 2011. https://doi.org/10.1016/j.dental.2011.03.007.

YAGHOOBINEZHAD, R.; AHN, J. J.; KANG, S. W. Chemical and microstructural characterization of two lithium disilicate glass-ceramics in the SiO2-Li2O-K2O-ZrO2 system. Journal of Non-Crystalline Solids, v. 505, p. 95-103, 2019. https://doi.org/10.1016/j.jnoncrysol.2018.11.008.

YANG, B. et al. Effects of surface treatments on the bonding to lithium disilicate ceramic: Shear bond strength and TEM analysis. Journal of Biomedical Materials Research, v. 77, p. 459-465, 2006. https://doi.org/10.1002/jbm.b.30438.

YU, L. et al. Influence of finishing/polishing on the flexural strength of lithium disilicate ceramics. Journal of Prosthetic Dentistry, v. 117, p. 267-274, 2017. https://doi.org/10.1016/j.prosdent.2016.08.013.

ZHANG, Y.; KIM, J. W.; BENZING, W. Flexural strength of dental lithium disilicate glass-ceramics after fatigue loading. Journal of Dental Research, v. 92, p. 292-297, 2013. https://doi.org/10.1177/0022034513475636.

APPENDICES

Table A1 - Means of the L*a*b* coordinates obtained for tempered lithium disilicate samples (untreated, polished, glazed) before and after thermal aging (white background).

Samples	**Before aging**			**After aging 10.000 cycles**		
No treatment (ST)	L*	a*	b*	L*	a*	b*
1	82.71	-1.72	9.84	82.51	-1.76	10.17
2	82.65	-1.85	9.77	82.46	-1.77	10.35
3	82.66	-1.81	9.82	82.67	-1.75	10.16
4	82.45	-1.77	9.94	82.25	-1.68	10.62
5	82.79	-1.72	9.80	82.32	-1.75	10.44
6	82.78	-1.79	9.63	82.32	-1.74	10.13
7	82.71	-1.70	9.89	82.55	-1.68	10.34
8	82.66	-1.81	9.58	82.41	-1.73	10.15
9	82.66	-1.75	9.81	82.31	-1.77	10.27
10	82.66	-1.70	9.99	82.66	-1.78	10.06
Average	82.67 ±	-1.76 ±	9.81 ±	82.45 ±	-1.74 ±	10.27 ±
Polished (POL)	L*	a*	b*	L*	a*	b*
1	82.21	-1.71	10.22	82.28	-1.77	10.48
2	82.02	-1.75	10.18	82.27	-1.78	10.26
3	81.95	-1.76	10.18	81.77	-1.75	10.53
4	82.11	-1.68	10.39	82.16	-1.78	11.12
5	82.13	-1.76	10.19	82.33	-1.79	10.46
6	81.55	-1.59	10.45	81.58	-1.75	10.69
7	82.14	-1.68	10.40	82.06	-1.77	10.90
8	81.97	-1.75	10.13	81.32	-1.59	10.96
9	82.26	-1.73	10.11	82.23	-1.81	10.34
10	82.09	-1.81	10.10	81.57	-1.76	10.74
Average	82.04 ±	-1.72 ±	10.23 ±	81.96 ±	-1.75 ±	10.65 ±
Glazed (GLAZ)	L*	a*	b*	L*	a*	b*
1	81.44	-1.68	10.16	82.07	-1.74	10.47
2	81.94	-1.75	9.98	82.28	-1.82	11.24
3	82.24	-1.71	9.82	82.02	-1.74	11.29
4	82.52	-1.72	9.63	82.25	-1.84	11.06
5	82.19	-1.62	9.92	81.88	-1.71	10.73
6	82.35	-1.71	9.82	82.01	-1.73	9.99
7	82.04	-1.64	10.09	82.11	-1.82	10.23
8	82.22	-1.66	10.14	82.06	-1.77	10.62
9	82.08	-1.63	10.07	82.25	-1.74	9.91
10	81.92	-1.72	9.92	81.74	-1.79	10.33
Average	82.09 ±	-1.69 ±	9.96 ±	82.07 ±	-1.77 ±	10.59 ±

Table A2 - Means of the L*a*b* coordinates obtained for tempered lithium disilicate samples (untreated, polished, glazed) before and after thermal aging (black background).

Samples	**Before aging**			**After aging 10.000 cycles**		
No treatment (ST)	L*	a*	b*	L*	a*	b*
1	57.37	-1.99	-0.40	56.93	-2.03	-0.38
2	57.61	-1.99	-0.37	57.01	-2.02	-0.23
3	57.89	-1.97	-0.23	57.11	-2.01	-0.43
4	57.18	-2.00	-0.35	57.74	-2.01	0.11
5	57.25	-1.92	-0.08	56.87	-2.06	-0.17
6	58.04	-1.99	-0.30	56.59	-2.01	-0.38
7	58.85	-1.77	0.47	58.19	-1.87	0.03
8	57.50	-1.99	-0.47	56.77	-2.03	-0.35
9	57.81	-1.94	-0.05	56.96	-2.02	-0.21
10	58.12	-1.87	0.06	57.06	-2.03	-0.41
Average	57.74	-1.94	-0.17	57.15	-2.01	-0.21
Polished (POL)	L*	a*	b*	L*	a*	b*
1	56.60	-2.03	-0.40	57.21	-1.85	1.02
2	56.15	-2.04	-0.54	56.82	-2.03	-0.29
3	56.84	-2.00	-0.01	56.11	-2.06	0.14
4	57.30	-1.92	0.05	57.01	-2.13	0.43
5	56.44	-2.05	-0.23	56.31	-2.05	-0.15
6	57.46	-1.81	0.65	56.62	-2.02	0.28
7	56.31	-2.00	-0.16	56.32	-2.12	0.04
8	56.45	-1.97	-0.16	57.33	-1.85	1.03
9	56.56	-1.99	-0.26	56.52	-2.05	-0.35
10	56.24	-1.99	-0.14	56.09	-2.03	0.07
Average	56.58	-1.98	-0.10	56.65	-2.03	0.19
Glazed (GLAZ)	L*	a*	b*	L*	a*	b*
1	57.08	-1.91	-0.36	56.32	-2.04	-0.04
2	55.54	-2.00	-0.22	56.45	-2.01	-0.47
3	57.35	-1.88	-0.18	55.92	-2.03	-0.10
4	57.04	-1.87	-0.14	57.17	-2.07	0.36
5	57.37	-1.86	-0.13	57.06	-1.93	0.52
6	57.21	-1.87	-0.08	55.93	-1.95	-0.19
7	56.48	-1.98	-0.37	56.92	-1.95	0.19
8	57.14	-1.90	0.06	56.36	-2.03	-0.10
9	56.99	-1.98	-0.14	56.45	-2.02	-0.44
10	56.18	-2.00	-0.37	55.93	-2.01	-0.14
Average	56.75	-1.94	-0.18	56.51	-2.01	0.02

Table A3 - Means of color differences (ΔE_{00}), luminosity differences ($\Delta L'$), chroma differences ($\Delta C'$), and hue differences ($\Delta H'$) for the samples under different tested conditions, when measured on a white background, with associated standard deviation (SD).

Samples	**Before aging**				**After aging 10.000 cycles**			
No treatment	ΔE_{00}	$\Delta L'$	$\Delta C'$	$\Delta H'$	ΔE_{00}	$\Delta L'$	$\Delta C'$	$\Delta H'$
1	0.23	-0.24	0.24	-0.002	0.49	-0.43	0.58	-0.04
2	0.29	-0.29	0.23	0.17	0.61	-0.49	0.75	-0.07
3	0.28	-0.29	0.26	0.12	0.43	-0.28	0.57	-0.05
4	0.49	-0.49	0.36	0.04	0.85	-0.69	0.99	-0.25
5	0.18	-0.16	0.21	0.001	0.71	-0.62	0.84	-0.11
6	0.17	-0.16	0.06	0.14	0.56	-0.62	0.52	-0.06
7	0.26	-0.23	0.29	-0.05	0.58	-0.39	0.72	-0.19
8	0.25	-0.28	0.03	0.19	0.52	-0.54	0.54	-0.08
9	0.25	-0.28	0.23	0.05	0.63	-0.63	0.67	-0.06
10	0.33	-0.28	0.38	-0.07	0.38	-0.29	0.47	0.02
Average SD	0.27 ± 0.07	-0.27 ± 0.09	0.23 ± 0.11	0.06 ± 0.02	0.58 ± 0.14	-0.50 ± 0.15	0.67 ± 0.16	-0.08 ± 0.08
Polished (POL)	ΔE_{00}	$\Delta L'$	$\Delta C'$	$\Delta H'$	ΔE_{00}	$\Delta L'$	$\Delta C'$	$\Delta H'$
1	0.66	-0.78	0.61	-0.12	0.76	-0.67	0.88	-0.10
2	0.74	-0.93	0.58	-0.06	0.65	-0.68	0.68	-0.03
3	0.78	-0.99	0.59	-0.03	1.02	-1.18	0.93	-0.14
4	0.75	-0.83	0.69	-0.18	1.17	-0.79	1.51	-0.22
5	0.68	-0.81	0.59	-0.05	0.73	-0.62	0.87	-0.07
6	1.12	-1.39	0.79	-0.34	1.19	-1.37	1.08	-0.17
7	0.78	-0.80	0.77	-0.20	1.08	-0.89	1.29	-0.19
8	0.75	-0.98	0.53	-0.04	1.46	-1.62	1.29	-0.44
9	0.58	-0.69	0.51	-0.07	0.71	-0.71	0.76	-0.01
10	0.68	-0.86	0.53	0.04	1.29	-1.38	1.13	-0.18
Average SP	0.75 ± 0.14	-0.90 ± 0.19	0.62 ± 0.09	-0.11 ± 0.11	0.99 ± 0.27	-0.99 ± 0.36	1.04 ± 0.26	-0.16 ± 0.12
Glazed (GLAZ)	ΔE_{00}	$\Delta L'$	$\Delta C'$	$\Delta H'$	ΔE_{00}	$\Delta L'$	$\Delta C'$	$\Delta H'$
1	1.09	-1.50	0.54	-0.15	0.85	-0.88	0.86	-0.14
2	0.73	-1.01	0.39	-0.001	1.20	-0.66	1.64	-0.20
3	0.50	-0.71	0.23	-0.02	1.31	-0.93	1.66	-0.31
4	0.29	-0.43	0.04	0.04	1.10	-0.69	1.46	-0.14
5	0.57	-0.76	0.28	-0.17	1.06	-1.07	1.10	-0.23
6	0.43	-0.60	0.23	-0.01	0.69	-0.94	0.39	-0.03
7	0.71	-0.91	0.46	-0.18	0.72	-0.83	0.66	0.04
8	0.62	-0.72	0.51	-0.16	0.92	-0.88	1.02	-0.14
9	0.67	-0.86	0.44	-0.19	0.52	-0.69	0.32	0.01
10	0.72	-1.02	0.12	-0.02	0.96	-1.21	0.74	-0.022
Average SD	0.63 ± 0.21	-0.85 ± 0.29	0.34 ± 0.15	-0.08 ± 0.09	0.93 ± 0.25	-0.27 ± 0.09	0.98 ± 0.48	-0.12 ± 0.12